UCLA
UCLA Electronic Theses and Dissertations

Title
Control of an Active Magnetic Bearing-Rotor System

Permalink
https://escholarship.org/uc/item/3hn6f536

Author
Kang, Christopher

Publication Date
2014

Peer reviewed|Thesis/dissertation

eScholarship.org Powered by the California Digital Library
University of California

University of California
Los Angeles

Control of an Active Magentic Bearing-Rotor System

A dissertation submitted in partial satisfaction
of the requirements for the degree
Doctor of Philosophy in Mechanical Engineering

by

Christopher Sunghwa Kang

2014

© Copyright by
Christopher Sunghwa Kang
2014

Abstract of the Dissertation

Control of an Active Magentic Bearing-Rotor System

by

Christopher Sunghwa Kang

Doctor of Philosophy in Mechanical Engineering

University of California, Los Angeles, 2014

Professor Tsu-Chin Tsao, Chair

A common disturbance encountered in rotor operations is the sinusoidal disturbance caused by mass unbalance. This natural phenomenon imparts a force on the rotor with frequency equal to the rotor speed. To help regulate the rotor and reject this disturbance, many researchers have investigated the use of Active Magnetic Bearings (AMBs) and digital control as a viable replacement for the traditional rotary journal bearing. The non-contact nature of AMBs allows for greater speeds and opens the possibility for new applications. Stability is an important design consideration as is the ability to provide disturbance rejection for varying rotor speeds and over the rotor's operational range.

An internal model principle type controller is implemented in this dissertation for its premium on stability and straightforward design parameters of the controller characteristics. The plug-in structure provides narrow performance enhancements while minimally disturbing the underlying stability of the closed-loop system. The internal model is realized through cascaded notch filters which allows for intuitive design of the internal model. Stability can easily be satisfied through a filter design formulation. These control strategies are applied on an AMB-rotor system with great rejection performance.

The dissertation of Christopher Sunghwa Kang is approved.

Panagiotis D. Christofides

Tetsuya Iwasaki

James S. Gibson

Tsu-Chin Tsao, Committee Chair

University of California, Los Angeles

2014

Despite your best efforts,

look what I have done.

Table of Contents

List of Figures

List of Tables

Acknowledgments

First, I must thank my advisor Professor Tsu-Chin "T-C" Tsao. Without his guidance, his wisdom, and his endless patience I would not be here today. He gave me a chance in his lab for which I will forever be in his debt.

I would also like to thank my committee members Steve Gibson, Tetsuya Iwasaki, and Panagiotis Christofides for their support and encouragement.

To my colleagues in the Mechatronics and Controls Laboratory at UCLA, of which there are many, my heart-felt appreciation. Yigang Wang, Shalom Ruben, Kevin Chu, Chris Lim, Jason Wilson, Stephen Prince, Herrick Chang, David Luong, Yen-Chi Chang, Kuo-Tai Teng, Ryan Beech, Rashid Yasin, James Simonelli, Niloufar Esfandi, Sandeep Rai, Grant Cavalier, Chengwei Chen, Matt Gerber, Martin Lee, and David Walter all made coming to work enjoyable and without any dull moments. Special thanks to Kevin and Stephen, who took me under their wing and cared enough to put me through my growing pains. Herrick always shared his insights, academic and otherwise, and for that I am grateful. Taiger, thanks for letting me bug you with ideas and questions. James and Sandeep, thanks for putting up with my nonsense and giving me some release.

Also to Nolan Tsuchiya who became a good friend and research collaborator despite sharing a desk with me for a whole summer.

My best friends Jae Kim, Mike Kim, Ray Kim, and Michael Marzouk were always available with words of encouragement or a beer; whatever I needed most. I'm not the kind of person who gets best friends - I am eternally grateful.

My sisters, Jessica and Jaime deserve my gratitude as well for their love and friendship which has helped me maintain my perspective and focus.

My parents and grandparents sacrificed so much of their lives for me. I am grateful more than I can show. An MD was their dream; I hope a PhD will suffice.

Vita

2007	B.S. (Mechanical Engineering), University of California, Berkeley, Berkeley, CA.
2008	M.S. (Mechanical Engineering), University of California, Los Angeles (UCLA), Los Angeles, CA.
2009-2014	Teaching Assistant, Mechanical and Aerospace Engineering Department, University of California, Los Angeles (UCLA), Los Angeles, CA
2010-2014	Graduate Student Researcher, Mechanical and Aerospace Engineering Department, University of California, Los Angeles (UCLA), Los Angeles, CA

Publications

C.Kang and T.-C. Tsao, "Control of Magnetic Bearings with Plug-In Time-Varying Harmonic Resonators," in *Proceedings of the 2014 American Control Conference*, June 2014, pp. 4237-4242.

CHAPTER 1

Introduction

1.1 Active Magnetic Bearing-Rotor Systems

A well-known problem affecting spinning rotors is that of rotor unbalance [SBT94]. Caused by mass imperfections in the shaft, this results in a periodic disturbance force synchronous to the rotor's angular velocity. In traditional rotor systems, the rotor is supported by journal bearings which are fit snugly over the outer diameter of the rotor. The unbalance force causes mechanical wear in the bearings as well as the force to be transmitted into the rotor housing.

An Active Magnetic Bearing (AMB) is a series of electromagnets arranged in a circular configuration capable of fitting over the outer diameter of the rotor and providing a non-contact force on it. Early uses of the AMBs were as a supplement to the system as a vibrational dampener [CDD94]. With the ends of the rotor fixed inside the mechanical bearings, a ring of electromagnets could be placed at set positions along the rotor length. Though effective, the problems remained that the rotor was still in contact with the stator and housing through the bearing.

AMBs are also used to replace the mechanical bearings and support the rotor by means of magnetic levitation. Magnetic levitation allows the bearing to be completely contact-less, which eliminates the issue of mechanical wear and friction, allowing the rotor system to be operated at higher speeds [BLP99]. Example applications include such systems as power generation [SL09], flywheels [CJL10], mills [ZSL03], and even on the impeller of an artificial heart [HST06].

Challenges associated with utilizing AMBs include their robust feedback control requirement as they are open-loop unstable [SBT94]. Furthermore, as AMBs do not rigidly support the rotor, they are susceptible to runout and other disturbances.

1.1.1 Rotor Unbalance

Rotor unbalances are distinguished between static and dynamic unbalances [TD98]. Static unbalance occurs when all the mass unbalance is restricted to one plane and can easily be remedied by adding counterweights to the disk. Modeling the rotor as a series of disks, dynamic unbalance occurs when each disk has its own offset center of mass. When stationary, the rotor may be statically balanced. However, dynamic unbalance can only be detected while the rotor system is spinning as it manifests as a sinusoidal inertial force on the rotor.

The net effect of dynamic rotor unbalance creates an inertial axis which is skew from the geometric axis of a cylindrical rotor. This has produced two schools of thought: 1) auto-balancing (or unbalance compensation) which allows the rotor to spin about its inertial axis of rotation, and 2) regulation which aims to force the rotor to spin about its geometric axis. Auto-balancing is attractive in an energy sense as it allows the system to operate at some stable steady-state set point and providing only necessary corrections. Some approaches include determining conditions off-line and applying feedforward control [KHF95, KHT96]. Notch filters have also been used in feedback control, though care must be taken to maintain stability of the closed loop system [HBG96].

However, unbalance compensation is not appropriate in all applications. For example, in machining operations the tool or workpiece must spin about its geometric axis to ensure accurate cuts and finish. In some operations, safety considerations may dictate that the rotor stay centered, relative to the stator, to prevent

any accidental collisions.

The focus of this research is the regulation problem on an AMB-rotor system.

1.2 Previous Research

In AMB-rotor systems, some important control design criteria exist. Primarily due to safety concerns during high rotor speed operations, robust control strategies must be employed. If the rotor were to make contact with the stator of housing while spinning at high velocities, the collision could be damaging to the system as well as dangerous to operators nearby. Strategies must also be effective for changing rotor speeds over the entire operating range. Robust feedback control implementations include a simple lead-compensator [AJE06], Linear-Quadratic-Gaussian control [YXS07] and linear parameter varying state-feedback scheduled on the rotor speed [LCB08].

To eliminate the unbalance vibration, sinusoidal internal models were used to augment the system and provide disturbance rejection [MFO89, BL00]. With the rotor stabilized with Proportional-Integral-Derivative control, an adaptive filter was able to identify and eliminate the harmonic disturbance [BLP99]. Linear parameter varying control was used to design controllers scheduled on the rotation speed [BWS12]. Disturbance observers were used to identify and compensate disturbances on a rotor during profile tracking [GL07].

When the rotor speed changes, and with it the disturbance period, the controller must be able to track and compensate for this. Altering the feedback loop has consequences to the stability of the system; which is highly dangerous for AMB-rotor systems. In the robust framework of H_∞ controllers, loop shaping filters for harmonic rejection were considered time-varying rotor speeds [MNH96, SNF06]. An adaptive scheme was used to identify parameters of the internal model during operation [LCR05].

Another internal model principle base controller, repetitive control is well-suited for the asymptotic tracking and rejection of harmonic signals. Researchers have studied various schemes on an AMB-rotor systems for disturbance rejection [ZSL03, THD07, PDA09].

1.3 Main Contributions

The goal of this research is to examine an internal model principle based controller for sinusoidal disturbance rejection on an AMB-rotor system for both constant and time-varying rotor speeds. The internal models are generated using peak filters and utilized in a plug-in structure [WCT09b]. The plug-in structure allows the stability criteria to be easily met through designing a robust feedback controller. The internal model controller narrowly enhances the performance of the closed-loop system, which can be controlled through intuitive design parameters.

The plug-in resonator also consists of a model inversion to provide nominal stability. The accuracy of this inversion conditions the internal model control signal, whereby a more accurate inversion will produce better rejection performance. Due to the non-minimum phase zeros present in the plant models, a couple standard approximate inversion techniques were applied.

In another technique, an FIR filter was also used to approximate the direct inversion of the non-minimum phase zero. This was at the expense of a large non-causal preview requirement. In the repetitive control framework, this preview cost is easily accommodated. Furthermore, the resonator was combined with repetitive control techniques to provide aggressive performance while simultaneously mitigating inter-harmonic amplification common in repetitive control.

A more accurate multivariable plant model was used for control design to improve performance. Though a multivariable model inversion is more difficult, the plug-in resonator derivation only requires the inversion to hold at discrete

points in the spectrum. An FIR filter was found to perform the stable inversion.

Though the plug-in resonator is well-suited for periodic disturbances, it is unable to handle more complex disturbances. In a collaborative effort, an adaptive filter was designed to reject the broadband components of a disturbance while the resonator remains in the plug-in configuration to this control loop for sinusoidal rejection. The controllers are integrated such that each filter can be independently designed on the pre-stabilized loop without coupling effects.

These controllers were designed and implemented on the MBC 500 Turbo, an AMB-rotor system by Launchpoint Technologies.

1.4 Outline

The remainder of this dissertation is organized as follows: the experimental system will first be described and discussed in Chapter 2. The modeling results will motivate much of the subsequent design and analysis. In Chapter 3, the plug-in resonator is introduced and discussed. The model inversion in the controller formulation is motivated through a stability argument and a couple traditional approaches are implemented. Chapter 4 is motivated by the more accurate inversion of the non-minimum phase systems. This cost of this inversion is easily accommodated by repetitive control. This is further improved through the incorporation of the internal models used in Chapter 3. The more accurate multivariable models of the system are used in Chapter 5 to design a MIMO version of the plug-in resonator. The model inversion is more easily accomplished by using an FIR filter to only invert the model at relevant points. In a collaborative effort, a more complex disturbance is rejected using both an adaptive filter and the plug-in resonator in Chapter 6.

CHAPTER 2

System Hardware and Modeling

2.1 Experimental System

Experimental results were obtained on the MBC 500 Turbo, an AMB-rotor system developed by LaunchPoint Technologies [PMS96]. The system consists of a rotor of 303-stainless steel supported at each end by electromagnets. Hall Effect sensors, collocated at each end, measure the gap distance to the rotor and provide positional feedback. The Turbo edition features a shortened shaft designed to push the resonant modes of the system past the maximum rotor speed.

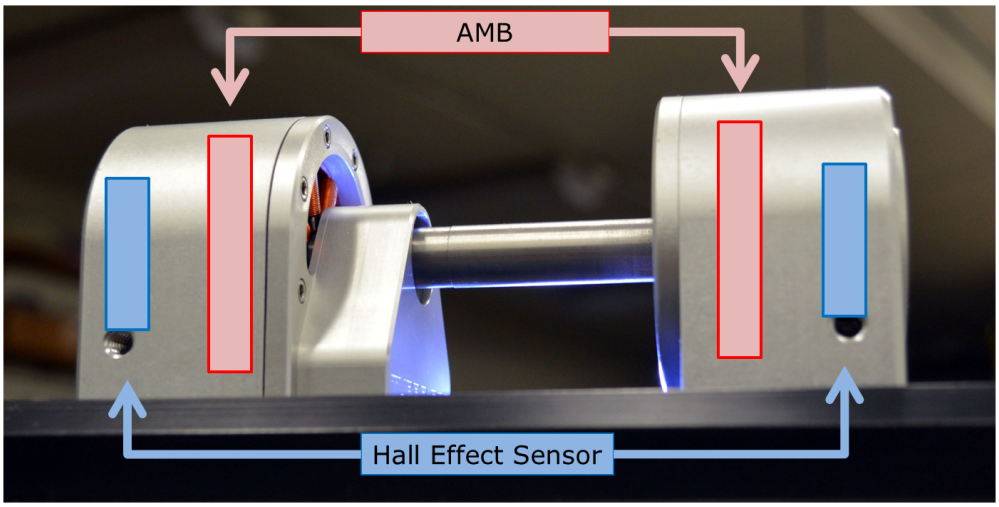

Figure 2.1: Actuator-Sensor placement of MBC 500 Turbo

At each end of the rotor (side-1 or side-2), actuation and sensing are conducted in the X-plane and the orthogonal Y-plane. In this coordinate system, they are

referred to as x_1, x_2, y_1 and y_2 directions. It is apparent that the system is a 4-input 4-output MIMO system. Motion along the axis (z) is constrained passively and assumed to have no effect on the dynamics of the system.

2.1.1 Hardware Implementation

Data acquisition and control were implemented using the Mathworks xPC Target platform at a sampling frequency of 10kHz. National Instruments PCI-6052e cards with 16-bit resolution were used for data acquisition and command. A PCI-6601 timer card with a 20MHz clock was used to measure the encoder period. A shaker table was installed to introduce additional disturbances to the system as appropriate.

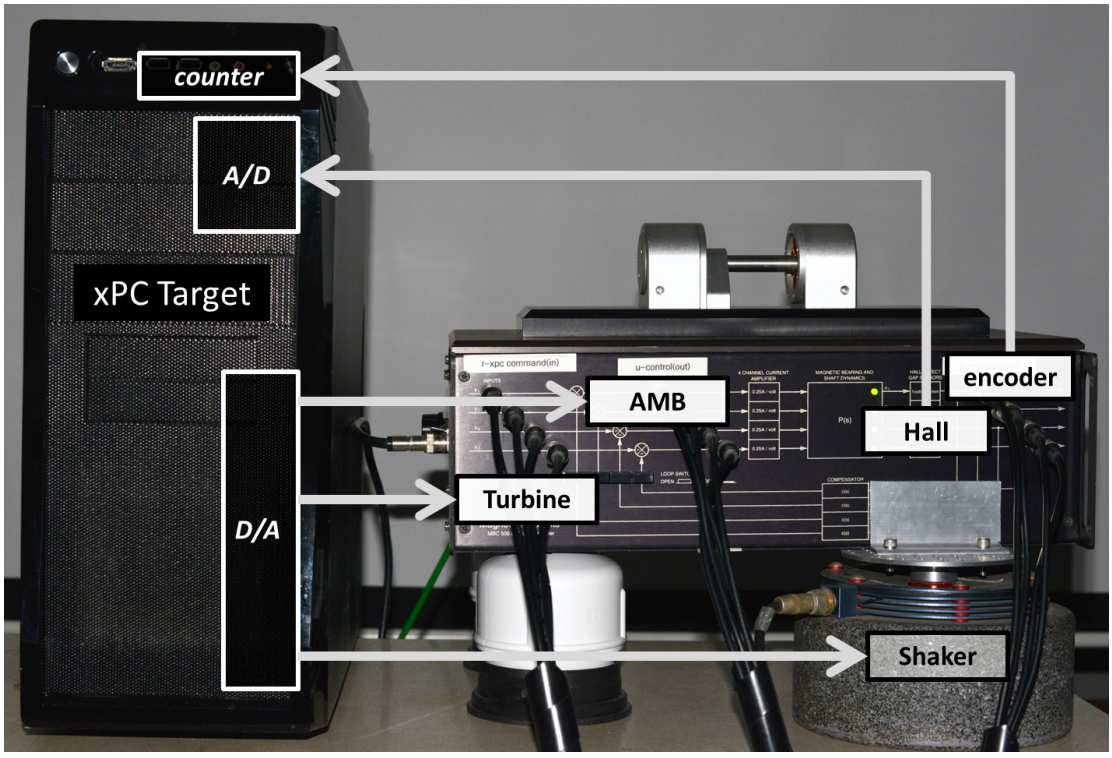

Figure 2.2: Experimental System Setup

2.2 Modeling

For the purpose of controller design, analysis, and simulation, models were developed for the MBC 500 Turbo [CWW10]. An analytical first-principles model provides the justification for decoupling and simplifying the model. To fully capture the electronic components, a closed-loop system identification was also performed.

The equation of motion, for a rigid shaft with the sensor-actuator configuration as described, can be written to produce a coupled 4-input 4-output model; two inputs per axial plane. For a relatively thin rotor, the gyroscopic elements will be small, decoupling the X-plane dynamics from the Y-plane. Furthermore, from geometric motivations, a coordinate transformation from the rotor-end coordinate frame to the geometric center further decouples motion in each plane.

$$\begin{pmatrix} x_T \\ x_R \end{pmatrix} = \begin{bmatrix} \frac{1}{2} & \frac{1}{2} \\ \frac{1}{2} & -\frac{1}{2} \end{bmatrix} \cdot \begin{pmatrix} x_1 \\ x_2 \end{pmatrix} \tag{2.1}$$

To more fully capture the other system components (e.g. electromagnets, A/D), a system identification procedure was performed. The open-loop instability of the system required a closed-loop method, with a secondary step to back out the open-loop data. Applying the decoupling transformation on the collected data, transfer functions could be fit to produce open-loop models of the four decoupled SISO systems. The decoupled SISO systems $[X_T\ X_R\ Y_T\ Y_R]$ correspond to the *Translational* and *Rotational* coordinate of the geometric center of mass in the X and Y planes. The data was also used to fit models to the uncoupled or raw coordinate frame.

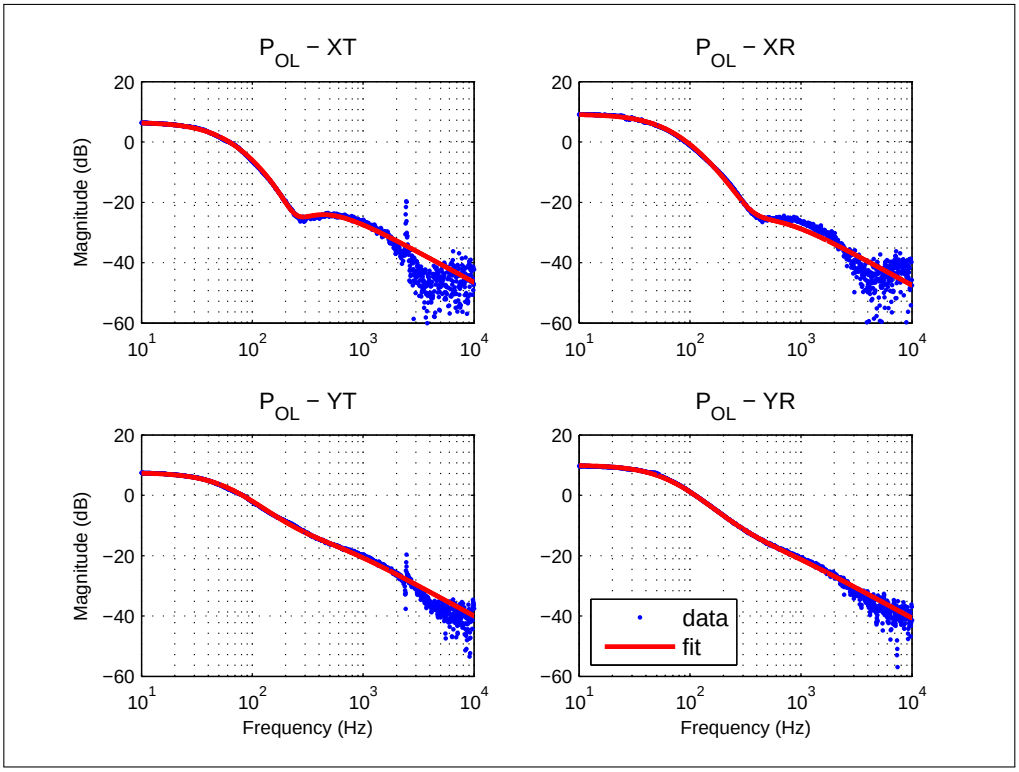

Figure 2.3: Model Fit of Decoupled Open-Loop Systems (Magnitude)

Figures 2.3 and 2.4 shows the collected frequency response data compared to the low-order fitted models. It is important to note the presence of a resonant peak in the two translational axes. The peak occurs near 2.5kHz and is not captured by the low-order transfer function. Higher order coupled models used for simulation capture this peak.

Continuous time 3^{rd}-order models satisfy physical intuition; two states describe motion of the rotor while the electromagnet contributes an unstable pole.

$$\begin{aligned} P_{XT} &= \frac{266.9(s^2 + 2126s + 5.47 \times 10^6)}{(s + 2479)(s + 442.8)(s - 460.9)} \\ P_{XR} &= \frac{298.8(s^2 + 942.2s + 2.46 \times 10^6)}{(s + 2240)(s + 394.6)(s - 392.7)} \\ P_{YT} &= \frac{-632.6(s - 1720)(s + 1252)}{(s + 3602)(s + 401.6)(s - 396.2)} \\ P_{YR} &= \frac{-583.6(s - 2639)(s + 1694)}{(s + 4196)(s + 438.3)(s - 447.8)} \end{aligned} \tag{2.2}$$

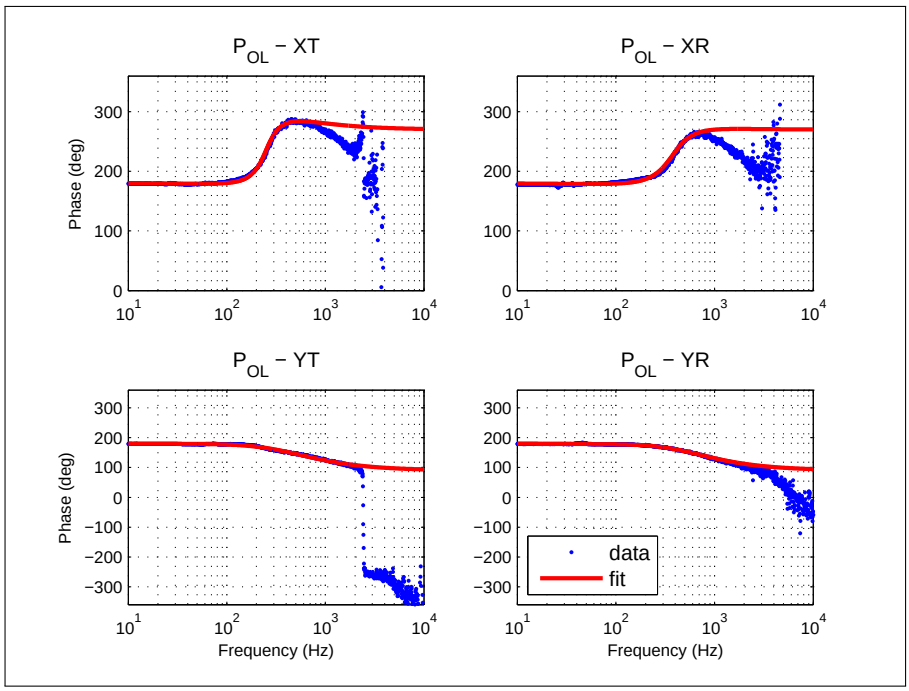

Figure 2.4: Model Fit of Decoupled Open-Loop Systems (Phase)

In each of the identified Y-plane systems, there exists one non-minimum phase zero. This will motivate much of the filter design considerations in subsequent sections.

2.2.1 Model Uncertainty

Due to the safety concerns of AMB-rotors operating at high speeds, any controller developed must prove a measure stability. The Robust Stability Criterion is a classic result through the Small Gain Theorem, where if the Complimentary Sensitivity Function T satisfies

$$|T| \leq \frac{1}{|\Delta|} \tag{2.3}$$

the system is robustly stable. Assuming multiplicative modeling error of the plant model $P_\Delta = (1 + \Delta)P_0$, the model uncertainty is defined by

$$\Delta = \frac{P - P_0}{P_0} \tag{2.4}$$

where P_0 is the nominal plant model [ZD98].

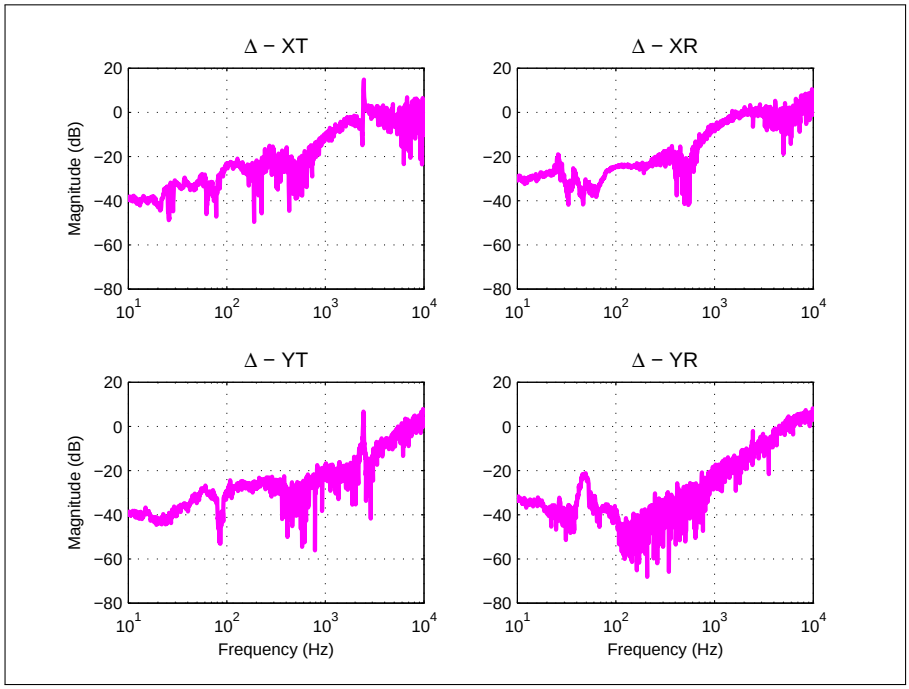

Figure 2.5: Multiplicative Modeling Error (Δ) of Decoupled Plants

The magnitude of the model uncertainty is shown in Figure 2.5 which shows higher uncertainty at higher frequencies. This is expected behavior for physical systems as they tend to exhibit low-pass behavior and will corrupt the identified data with noise.

2.3 Feedback Control

AMB systems are open-loop unstable and require a feedback controller for operation. Though designing feedback control strategies can be effective, one purpose of this work is to demonstrate the benefits and performance achievable implementing a plug-in control module. This is motivated by the fact that in most systems, some feedback controller will already by designed and implemented. An effective complimentary controller can be designed without disturbing the pre-stabilized

system. Thus the feedback controller was designed to provide good stability margins and low broadband authority without too much emphasis given to extracting performance.

The MBC500 Turbo system is equipped with four analog Proportional-Derivative (PD) controllers. They were replaced in favor of LQG with integral action (LQGi), to provide stable and robust levitation over the entire operating speed range. Integral action was included to center the rotor in relation to the stator housing to prevent collisions between the rotor and housing.

2.3.1 LQGi Control Design

The state-space controller LQGi is a specific method of state-estimator feedback using the combination of a linear-quadratic regulator with integrator (LQR) and a Kalman filter (a linear-quadratic estimator) for state estimation of the system. For the state-space representation of the system augmented with an integral state

$$\bar{x}(k+1) = \begin{bmatrix} x(k+1) \\ x_i(k+1) \end{bmatrix} = \begin{bmatrix} A & 0 \\ -C & 1 \end{bmatrix} \bar{x}(k) + \begin{bmatrix} B \\ 0 \end{bmatrix} u(k) \tag{2.5}$$

$$y(k) = \begin{bmatrix} C & 0 \end{bmatrix} \bar{x}(k)$$

the optimal state-feedback controller given by $u = -\bar{K}\bar{x}(k)$ minimizes the quadratic cost function

$$J_{lqi} = \sum_{k=0}^{\infty} \bar{x}^{\top}(k) Q \bar{x}(k) + u^{\top}(k) R u(k) \tag{2.6}$$

$$Q = \begin{bmatrix} C^{\top}C & 0 \\ 0 & q_i \end{bmatrix} \quad R = \rho_u$$

where Q and R are square symmetric weighting matrices on the states and control effort respectively. R is positive definite while Q is allowed to be positive semi-definite. A typical choice of weighting matrices are used for the SISO

case where q_i and ρ_u are scalar weights for the integral state and control effort, respectively.

A closed form expression for the optimal controls gains $\bar{K}$ is defined as

$$\bar{K} = (R + B^\top PB)^{-1} B^\top PA \tag{2.7}$$

where P is found by solving the steady-state discrete-time algebraic Riccati equation

$$P = A^\top (P - PB(R + B^\top PB)^{-1} B^\top P)A + Q \tag{2.8}$$

The Kalman estimator provides the estimates states which minimizes the error covariance. To make a similar optimal argument, another quadratic cost function is defined

$$J_{kal} = E\Big[\Big[e(k) - E[e(k)]\Big]\Big[e(k) - E[e(k)]\Big]^\top\Big] = M \tag{2.9}$$

where M is the state-error covariance, e is the error and the notation $E[\cdot]$ denotes the expected value of the arguemnt. The states estimates are updated by

$$\hat{x}(k+1) = \hat{x}(k) + L[y(k) - C\hat{x}(k)] \tag{2.10}$$

which is essentially the best linear combination of the current measurement and model propagation to minimize (2.9). The optimal Kalman gains which achieve this is defined as

$$L = AMC^\top (CMC^\top + R_n)^{-1} \tag{2.11}$$

where M is found by solving another discrete-time Ricatti equation

$$M = A(M - MC^\top (CMC^\top + R_n)^{-1} CM)A^\top + Q_n \tag{2.12}$$

The sensor noise and process noise covariances, R_n and Q_n respectively, are used to characterize aggressiveness of the estimation.

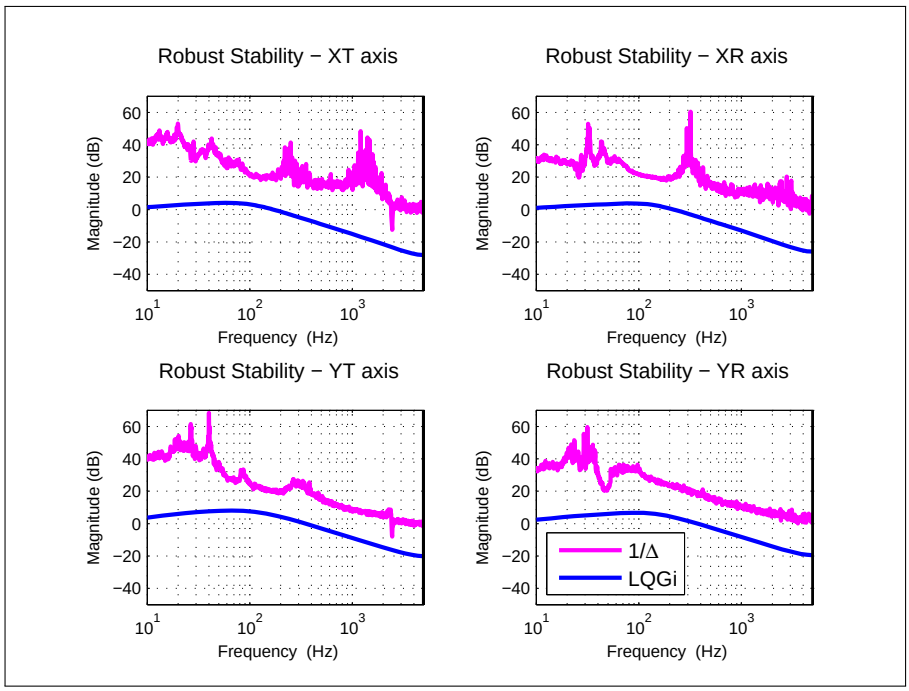

Figure 2.6: Robust Stability Analysis of Feedback Controller

An LQGi feedback controller was designed for each of the decoupled systems. Robust stability can be verified from (2.3) and shown in Figure 2.6 to easily satisfy the criteria with sufficient margins.

2.3.2 Experimental Results

The designed LQGi feedback controller was implemented on the experimental system and measurements collected to establish a baseline performance.

Figure 2.7 is a time trace of the X-Translation of the rotor during two constant rotor speeds of 200Hz and 0Hz. It illustrates the loss of regulation performance due to the large sinusoidal disturbance. This can be further quantifies by evaluating the RMS of the error and organized in Table 2.1 for all the coordinates. The measurements are converted into units of displacements; microns from translation and micro-radians for rotation. The feedback controller is successful in maintaining stability but is unable to reduce much of the harmonic disturbance.

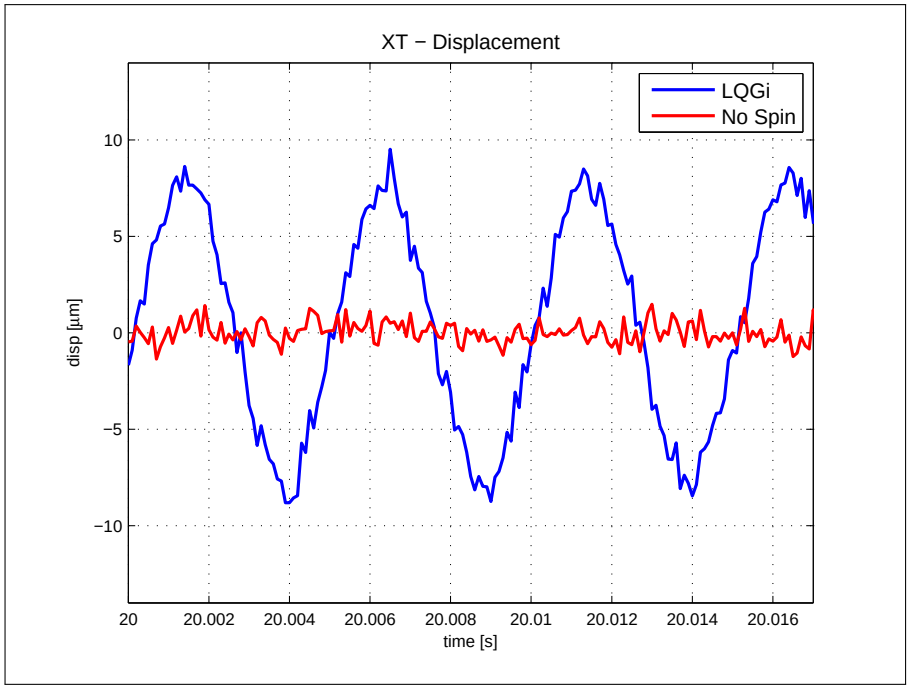

Figure 2.7: Rotor Disp. - X-Translation under LQGi

RMS	XT [μm]	XR [μrad]	YT [μm]	YR [μrad]
LQGi	5.57	1512.41	10.75	2730.2
No Spin	0.59	88.68	0.84	112.7

Table 2.1: RMS Error - Feedback Controller

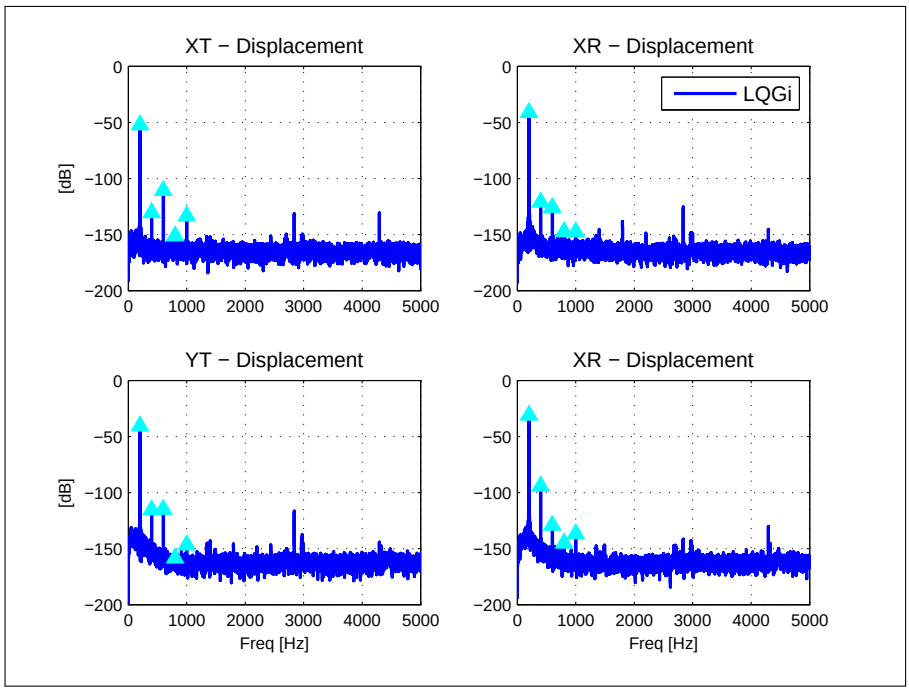

Figure 2.8: Spectrum - LQGi Feedback Control

From spectral analysis in Figure 2.8, sharp harmonic components can seen. These correspond to the rotor speed and its first four integer overtones. A few high-frequency components also exist. The component near 3kHz is thought to be vibrations from the onboard electronics fan and not the resonant mode from the modeling discussion. Under LQGi, the majority of the spectrum is at or near the noise floor. The narrow disturbance components support the approach of utilizing narrowband internal models for disturbance rejection.

2.4 Rotor Speed Sensing and Control

Controlling the speed of the rotor is an important aspect of the experiment to the extent that repeatability of the process is required. More relevant yet is to consider that the peaks of the internal model can easily be placed at any frequency. An important aspect then is to place them appropriately, which entails correctly identifying the disturbance period. In the case of rotor unbalance, this

problem can be viewed as determining the speed of the rotor. Two approaches were explored and is discussed in this section.

2.4.1 Encoder Measurement

In many rotor-based systems, a common method is to use a sensor to measure the rotor speed. A tachometer or rotary encoder are easily implemented. The MBC 500 Turbo is equipped with a low resolution (two counts/rev) quadrature encoder. In essence, the rising edge of each encoder channel indicates one complete revolution of the rotor. The pulses of a channel are used to trigger the PCI-6601 high clock rate (20MHz) timer card. This returns the period of each encoder pulse and thus a measure of the rotor speed. The measured speed is used to close the loop on a Proportional-Integral-Derivative (PID) controller for servo valve command.

Furthermore, stiction was observed to cause hunting of the speed set point, preventing the rotor from reaching any useful constant speed. To counteract stiction in the servo valve, a high-frequency zero-mean dither signal was added to the valve command. Sample regulation behavior in Figure 2.9 shows the improvement in velocity tracking with and without stiction.

2.4.2 Online Adaptive Frequency Estimation

In the event that such hardware is not available or a possible option, online frequency estimation can be used for disturbance rejection. For fast convergence and stable estimate, an adaptive notch filter formulation was used to determine the frequency of rotor unbalance [Li97, WCT09a]. A brief description follows.

The adaptive filter N is a constrained notch filter with zeros on the unit circle

$$N = \frac{1 - 2\cos\theta z^{-1} + z^{-2}}{1 - 2\alpha\cos\theta z^{-1} + \alpha^2 z^{-2}} \tag{2.13}$$

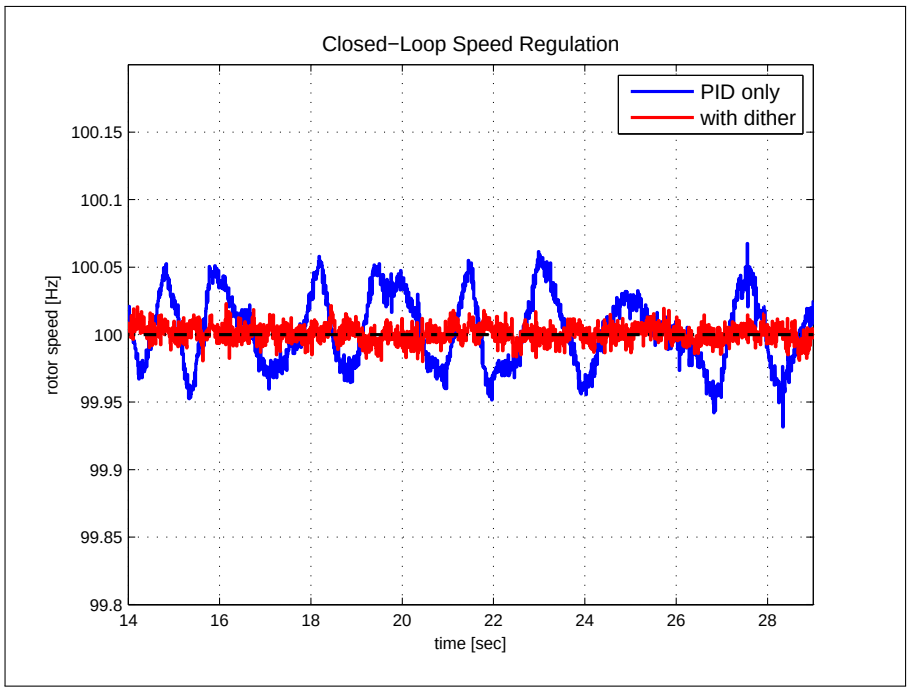

Figure 2.9: Rotor Speed Regulation Improvement with Dither Signal

The cost function is defined as

$$J(\theta, t) = \frac{1}{2t} \sum_{n=1}^{t} \hat{v}^2(\theta, t) \tag{2.14}$$

where $\hat{v} = Ny$ is the filter output to an input signal. The estimate is found recursively using a gradient descent search.

The adaptive filter is placed as shown in Figure 2.10. Instead of feeding the output of the plant directly, a model of the closed-loop system is used to produce an output estimate $\hat{y}$. This can be used to estimate the disturbance signal which provides a more robust signal to estimate the disturbance frequency.

A comparison between the two methods are made for two important rotor conditions in Figure 2.11.

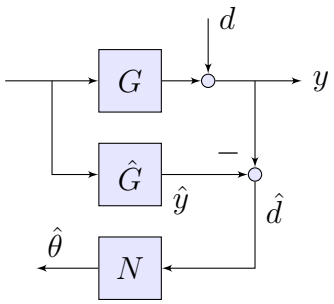

Figure 2.10: Block Diagram of Adaptive Filter Implementation

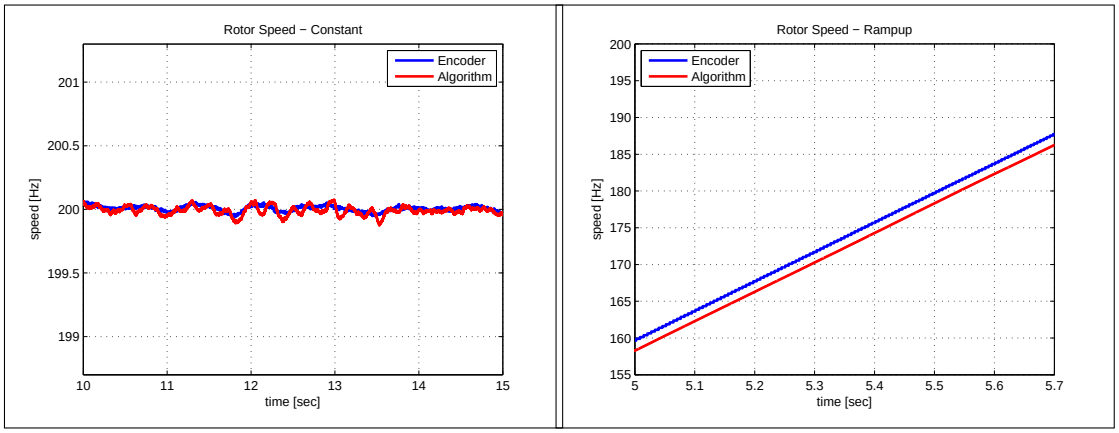

(a) Constant Speed **(b)** Varying Speed

Figure 2.11: Rotor Speed Identification Methods

When the desired speed is constant, both methods produce accurate identifications. The algorithm contains more variations due to the additional harmonic components present in the measured output. Still, the accuracy in speed is within ± 0.1Hz which satisfies the precision necessary for use in the controller. When the rotor is changing accelerating however, the adaptive algorithm naturally lags behind the encoder due to the necessary number of data points which must be processed, posing a problem for applicability during these transition regions.

Certainly the plug-in controller could be designed for robustness to frequency mismatch. By adjusting the bandwidth of the peaks, the controller can be made to work for a variety of signal qualities. In the interest of simplifying the im-

plementation for both time-varying and constant speed operations, the encoder measurement will be used update the plug-in controller as well as to close the speed feedback loop.

CHAPTER 3

Plug-in Resonator

3.1 Introduction

Disturbance due to rotor unbalance can be modeled as a sinusoid with frequency synchronous with the rotor's rotational velocity. Furthermore, the rotor's speed may vary and thus requires the ability to keep track of it. Maintaining stability is critical in operating the AMB-rotor system safely. To that end, a plug-in internal model principle-based controller is proposed for the purpose of sinusoidal disturbance rejection [WCT09b, KT14].

The plug-in structure allows disturbance rejection of specific harmonic frequencies with minimal effect to the stability of the system. The resonator is generated through inversion of 2^{nd}-order notch filters, providing greater flexibility in tuning performance of the controller while being easily amenable to rotor speed changes. The following chapter will describe details of the control strategy, motivate a couple approximate model inversion methods, and provide experimental results on the system.

3.2 Resonator

The harmonic resonator is employed as a plug-in unit to a pre-existing feedback loop shown by the block diagram of Figure 3.1. The controller C_1 can be used to provide stability or satisfy other design criteria (e.g. LQGi), while the plug-in

controller C supplies targeted control effort. The closed-loop system, $G = \frac{PC_1}{1+PC_1}$, is used in the plug-in controller design.

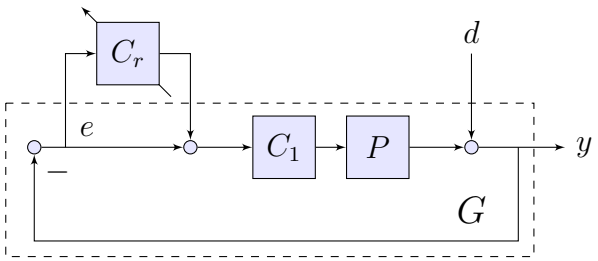

Figure 3.1: Block Diagram of Plug-in Controller C_r to Feedback System

The plug-in controller (C_r) is composed of two filters

$$C_r = D \cdot F \tag{3.1}$$

the internal model D and a stable inversion F.

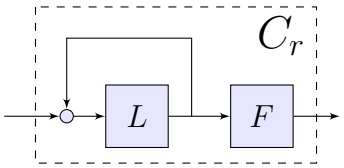

Figure 3.2: Components of Harmonic Resonator

3.2.1 Internal Model Design

The Internal Model Principle requires a model of the disturbance to be placed in the feedback path [FW76]. A filter L satisfying the criteria

$$L = \begin{cases} L = 1 \text{ if } \omega = \omega_{k=1,2,\ldots p} \\ L \approx 0 \text{ if } \omega \neq \omega_k \end{cases} \tag{3.2}$$

can be placed in a positive-feedback loop to produce infinite control gains at the p-number of interested frequencies, while remaining small elsewhere.

Filter L is realized by first designing a series of cascaded 2^{nd}-order notch filters defined by

$$H = \prod_{k=1}^{p} \frac{1 - 2\beta_k \cos \omega_k z^{-1} + \beta_k^2 z^{-2}}{1 - 2\rho_k \cos \omega_k z^{-1} + \rho_k^2 z^{-2}} \tag{3.3}$$

This formulation makes specifying key parameters of the internal model straightforward. The parameter ω_k in (4.6) represents the location of the notch in the Nyquist band and it is quite apparent that any frequency can be specified, including non-integer speeds. In general, the disturbance signal may be characterized by multiple frequencies which may not share any relative relationship among them (e.g. not harmonics). By cascading notch filters, (4.6) can provide compensation at the appropriate frequencies with the freedom of independently selecting these frequencies. By cascading them, the notch filters also minimally effect one another to present a near ideal series of notches.

Furthermore, by using this 2^{nd}-order notch filter as the basis, we can take advantage of the direct control over the characteristic of each notch. Parameters of the filter, ρ and β, shape the depth and bandwidth. They can be tuned independently for each k^{th} frequency. The two factors are chosen to satisfy the relationship $0 << \rho < \beta \leq 1$. For the notch filter, $\beta = 1$ places the zeros on the unit circle producing zero filter output. Once it is inverted, the peak is at unity and satisfies the criteria of (4.8) to produce infinite gain in the feedback loop. The parameter ρ controls radius of the poles of H. As $\rho \to 1$, the filter becomes more ideal in that frequencies away from the notch are less affected while $\rho < 1$ is maintained to keep the poles inside the unit circle to produce a stable filter.

The relationship between the two factors can be used to approximate the -3dB bandwidth in Hertz through the expression

$$BW_{Hz} \approx \frac{\pi(\beta_k - \rho_k)}{2\pi T_s} \tag{3.4}$$

where T_s is the sample time of the discrete time system. A wider notch provides faster convergence as well as robustness to mismatches between the disturbance

and controller frequencies. This must be balanced by the consequences of the so-called "waterbed effect," which describes the resulting amplification in another part of the spectrum resulting in a loss of performance and stability.

The peak filter is made by inverting the notch filter

$$L = 1 - H \tag{3.5}$$

In Figure 3.2, the internal model is generated by wrapping the peak filter in a positive feedback loop.

$$D = \frac{L}{1 - L} \tag{3.6}$$

3.2.2 Plant Inversion for Stability

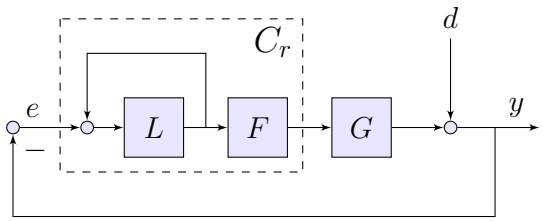

Figure 3.3: Simplified Block Diagram of Plug-In Resonator in Feedback

Filter F is motivated by a stability condition

$$\|L(1 - FG)\|_\infty < 1 \tag{3.7}$$

derived from a conservative enforcement of the Nyquist Stability Criterion and the block diagram of Figure 3.3. The encirclement criterion states that the open-loop gain must encircle the critical point (-1,0) the proper number of times for closed-loop stability. For stable filters L, F, and G, we require no encirclements. To guarantee this conservatively, the magnitude of the loop gain is restricted to remain inside the unit circle. If the contour never escapes the unit circle, it could never encircle the critical point.

The criterion in (3.7) is easily satisfied in the majority of the spectrum by the explicit design of L from (4.8). The condition in (3.7) then reduces to a filter design problem to satisfy

$$\|1 - FG^{-1}(e^{j\omega})\|_\infty < 1 \tag{3.8}$$

One approach to this design is to consider plant inversions.

For the minimum phase system of the X-plane, a complete model inversion is possible. However, recall from (2.2) the two Y-plane systems each had one unstable zero. A complete inversion for these systems would produce an unstable inversion, thus require approximate model inversion techniques..

3.2.2.1 Zero Phase Error Inversion Filter

A popular method of performing the non-minimum phase plant inversion is the Zero Phase Error Controller (ZPEC) which inverts the phase response at the expense of the magnitude [Tom87]. For a factorization of the stable system

$$G = \frac{z^{-d}B^+B^-}{A} \tag{3.9}$$

d represents the relative system order, and A, B^+, and B^- are the poles, stable zeros, and unstable zeros, respectively. The ZPEC inversion is defined as

$$F_{zpec} = \frac{A[B^-]^*}{\gamma z^{-d}B^+} \tag{3.10}$$

where $[B^-]^*$ is the complex conjugate of the unstable zeros. The accuracy of the inversion can be examined through their product, $F_{zpec}G = \frac{B^-[B^-]^*}{\gamma}$ which has zero phase since the zeros are complex conjugates of one another.

Though the phase is compensated, the magnitude response is inherited from the position of the unstable zeros. Non-minimum phase zeros near the unit circle results in a filter which generates high gains near the Nyquist frequency [BPA12]. To maintain stability, the constant $\gamma = [B^-(e^{jw})][B^-(e^{-jw})]$ is used to scale the

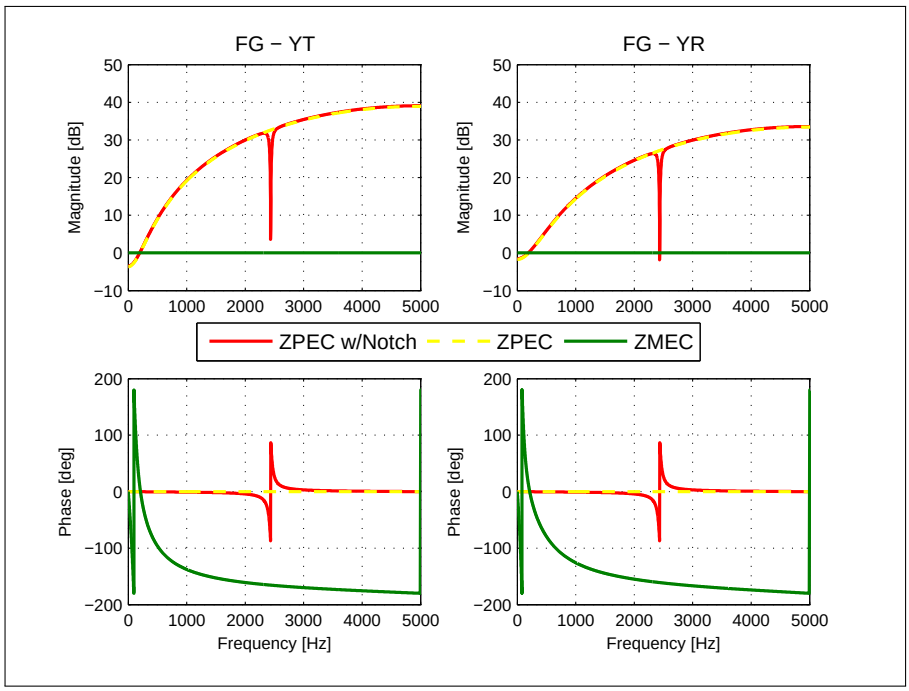

Figure 3.4: *FG* comparison for various F designs at 200Hz

magnitude of the filter output to unity at a prescribed frequency (Figure 3.4 (yellow)).

Despite the idealized design of L in (4.8), the high pass magnitude response of ZPEC was found to internally excite the resonant modes of the Translational systems identified in Section 2.2. A notch was designed to filter out the control component at 2.5kHz. As the feedback controller itself did not excite this mode, and to emphasize the utility of the plug-in approach on an inherited closed-loop system, the notch was placed in series with ZPEC in the plug-in controller to produce the notched-version of the inversion (Figure 3.4 (red)).

3.2.2.2 Zero Magnitude Error Inversion Filter

The unfavorable magnitude inversion of ZPEC leads to the examination of another approximate model inversion. The Zero Magnitude Error Control (ZMEC) is a similar approximate model inversion technique, though it will invert the mag-

nitude rather than the phase [RPL09]. The filter defined as

$$F_{zmec} = \frac{A}{z^{-d}B^{+}[B^{-}]^{*}} \tag{3.11}$$

produces the product $F_{zmec}G = \frac{B^{-}}{[B^{-}]^{*}}$ which is essentially an all-pass filter with unit magnitude. The magnitude response is more favorable as it does not cause any internal amplification. The phase however, must be compensated similar to the role of γ in ZPEC. An additional all-pass filter F_{ap}

$$F_{ap} = \frac{r^2 - 2\cos(\omega_{ap})z^{-1} + z^{-2}}{1 - 2\cos(\omega_{ap})z^{-1} + r^2 z^{-2}} \tag{3.12}$$

is designed and cascaded to adjust the phase. The corner frequency ω_{ap} determines where the phase is $-\pi$ and the parameter r affects the sharpness of the transition. By first determining the phase of $F_{zmec}G(e^{jw})$, the necessary phase compensation can be determined and an appropriate ω_{ap} can be calculated to provide compensation (Figure 3.4 (green)).

3.2.2.3 Causal Implementation

For strictly proper systems and/or those with non-minimum phase zeros, the resulting inversions will be non-causal. They must be provided with enough "look-ahead" or "preview" steps to form a causal filter. Separating into a causal filter and non-causal previews

$$z^{m_1}F_{zpec,caus} = z^{m_1}\frac{A[B^{-}]^{*}}{\gamma z^{(d+2n_u)}B^{+}} \tag{3.13}$$

$$z^{m_2}F_{zmec,caus} = z^{m_2}\frac{A}{z^{d}B^{+}[B^{-}]^{*}} \cdot F_{ap} \tag{3.14}$$

where n_u is the number of unstable zeros, $m_1 = d + n_u$ and $m_2 = d$ represent the preview requirement for each respective filter.

The positive feedback loop and relative order of L in the internal model can be exploited. Peak filter L has a relative order of one, allowing it to provide a

one-step preview. To compensate n-step previews, the underlying notch filter can be up-sampled to

$$H_n = \prod_{k=1}^{p} \frac{1 - 2\beta_k \cos n\omega_k z^{-n} + \beta_k^2 z^{-2n}}{1 - 2\rho_k \cos n\omega_k z^{-n} + \rho_k^2 z^{-2n}} \tag{3.15}$$

Then (4.7) would produce a peak filter with n-relative order. Thus, an n-step preview requirement can be compensated by the up-sampled filter and $L_n z^n$ will remain proper. However, directly applying (4.7) to produce L_m will cause $(m-1)$ aliased peaks to show up in the band at locations

$$\omega_{k,i} = \left| \left(\omega_k \pm \frac{2\pi i}{m} \right) \mod (2\pi) \right| \tag{3.16}$$

where $i \in \mathbb{Z}$ between $0 \leq i \leq \lfloor \frac{m}{2} \rfloor$. The aliased peaks are removed while maintaining the correct filter order by combining two filters such that for an m-step preview requirement

$$L_m = L_1 L_{(m-1)} \tag{3.17}$$

For a given system, F_{zmec} will require less lifting of L (i.e. only for relative order) and yield comparatively wider notches.

3.2.3 Stability and Sensitivity Analysis

Due to the importance of stability in AMB-rotor operations, stability analysis of the controller will be a main tool in the design process. One measure of stability, the criterion in (3.7) is verified. Nominally, a complete inversion of the X-plane plants can be found resulting in the left-hand side of (3.7) evaluating to 0. Thus, only the nontrivial results for the Y-plane systems are shown in Figure 3.5.

Though the unstable zeros result in high magnitudes for the ZPEC formulation, by using γ to scale the magnitude crossing, the L filter can work in tandem to satisfy the criteria. Likewise, the ZMEC formulation satisfies the stability criterion. In the transition between the two filters, the magnitude increase is

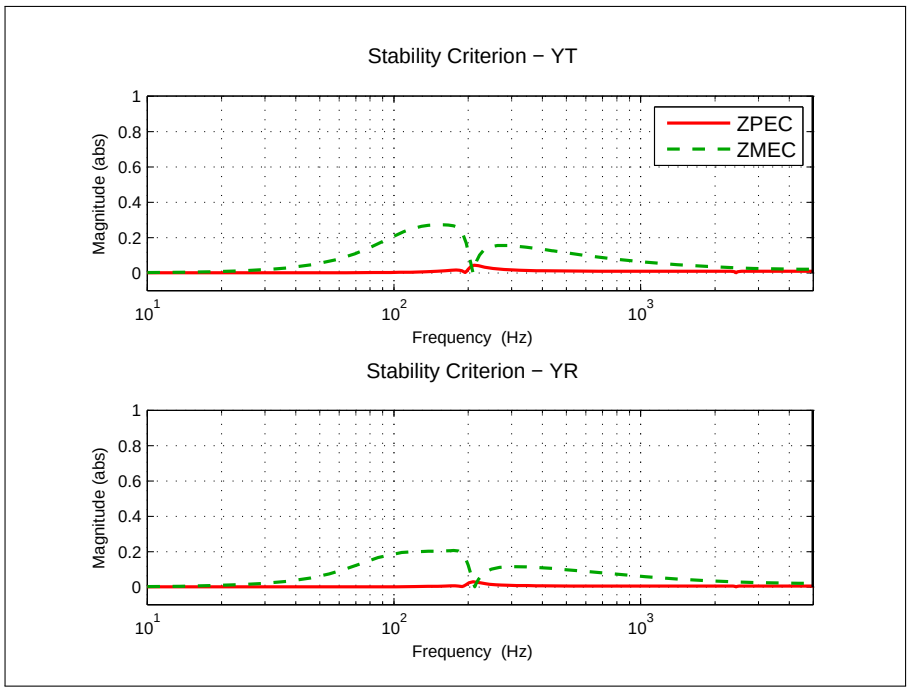

Figure 3.5: Stability Criterion (3.7) of Y-plane Systems

caused by the imperfect phase compensation in the transition band of the all-pass filter.

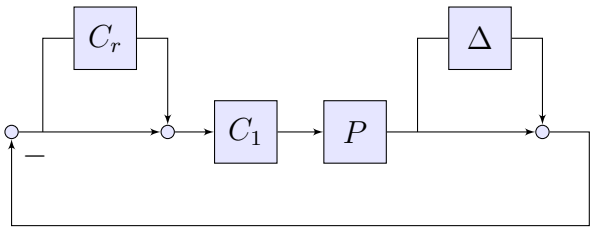

Figure 3.6: Block Diagram with Multiplicative Model Uncertainty for Robust Stability Analysis

The Robust Stability criterion is also verified from Figure 3.6 and (2.3) to produce the transfer function expression

$$T = \frac{C_1 P(1+DF)}{1+C_1 P(1+DF)} \tag{3.18}$$

$$\left| \frac{C_1 P(1+DF)}{1+C_1 P(1+DF)} \right| \leq \frac{1}{|\Delta|} \tag{3.19}$$

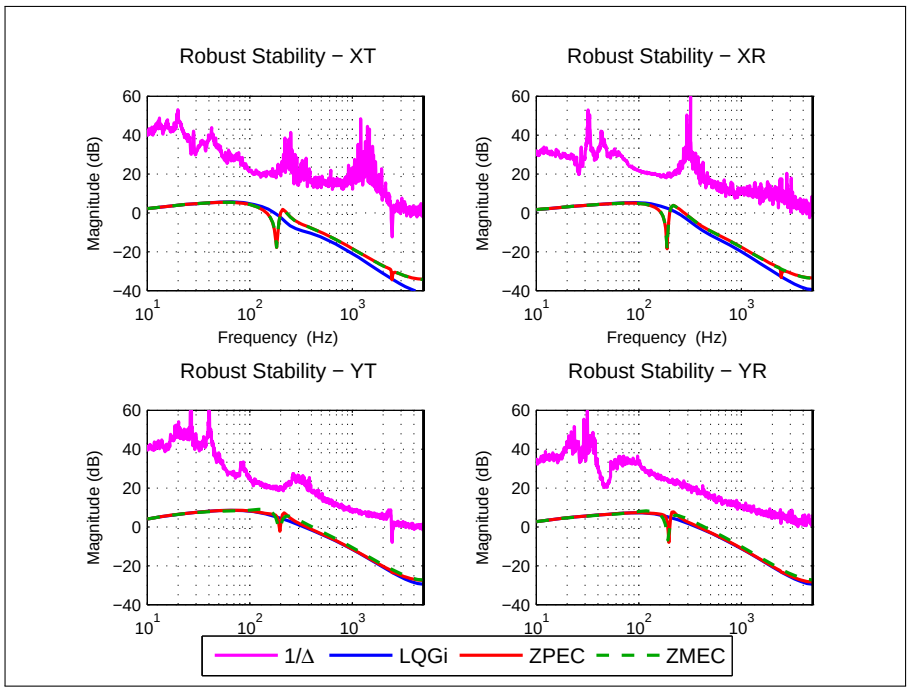

Figure 3.7: Robust Stability of Plug-In Resonators

The plug-in resonator with the approximate inversion methods described are shown to satisfy the stability criteria in Figure 3.7. The stability of the pre-stabilizing feedback controller is mainly preserved with the addition of the plug-in resonator. Only in the neighborhood of the designed peaks does the stability condition deviate from that of LQGi. For the ZPEC controller method, the dip at 2.5kHz indicates the inclusion of the control notch filter the the resonant mode is not excited.

Analysis of the sensitivity function can be insightful as a measure of expected performance. From Figure 3.1, the closed-loop sensitivity function can be evaluated to produce

$$S = S_{C1} \cdot S_{C_r} = \frac{1}{1 + PC_1} \cdot \frac{1}{1 + GC_r} \tag{3.20}$$

This factorization highlights the property of the plug-in structure where the sensitivity of the underlying pre-stabilized sensitivity S_{C1} is narrowly effected by the addition of the plug-in controller. Furthermore, the resonator C_r is designed using

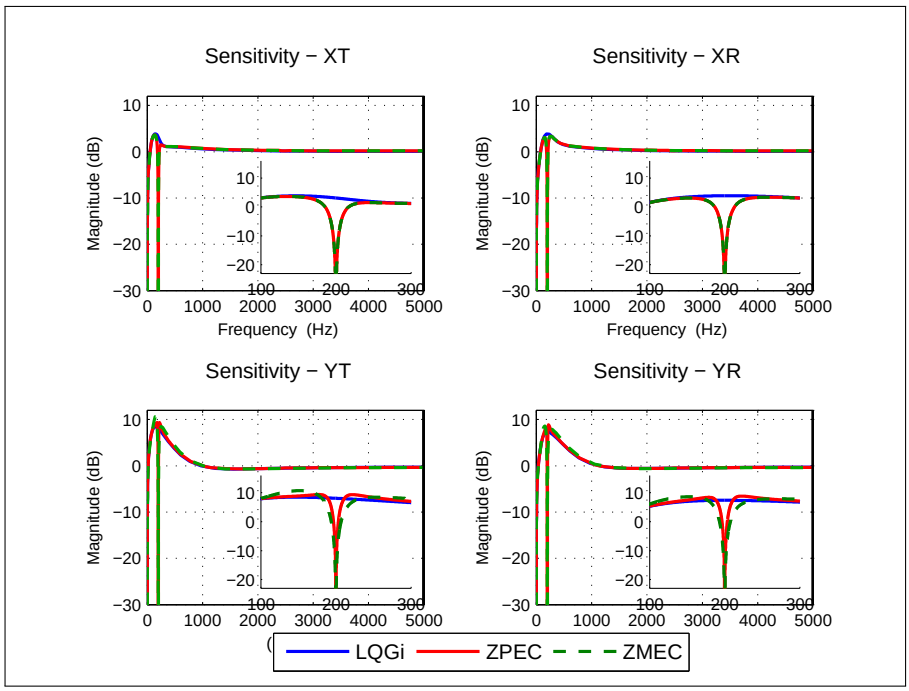

Figure 3.8: Sensitivity Analysis of Plug-In Resonators

only the closed-loop plant G.

Figure 3.8 compares the sensitivity functions for plug-in controllers designed using the inversion methods described. Again, in much of the spectrum, the transfer functions overlap greatly. As expected from (3.20), the sensitivity function of the closed-loop system is modified only at the designed frequencies. The plot inserts in each respective subplot highlights the effect of the peak resonator in reducing the sensitivity to disturbances in that band.

To ensure a fair comparison, the parameters of peak and inversion were chosen identically where appropriate. This is verified by the identical controllers for the X-plane systems. Since these systems are minimum phase systems, both inversions yield the same filter.

The differences in the Y-plane systems then, are a result of how each algorithm handles the unstable zero. Because the ZPEC method will always require more lifting, the resulting peak filter construction in (3.17) effectively narrows the

bandwidth for the same notch parameters. For a notch filter, the convergence can be determined by the parameter ρ, where a smaller ρ yields faster convergence [WWZ07]. In other words, a wider notch bandwidth results in faster convergence, as well as being more robust to a mismatch in the identified disturbance frequency. Consequently, a wider notch means more pronounced ripples in the spectrum. This is evident in the insert plots of the Y-plane system of Figure 3.8. The notch formed by ZMEC (green) is wider than ZPEC (red), while suffering from larger amplification (notch ripple) in the regions near the notch.

It should be noted that it is more challenging to design a satisfactory ZMEC filter. Since the all-pass filter for frequency compensation must be designed to correct the phase at each targeted frequency, multiple all-pass sections may be required. The addition of each filter, will affect the phase of the previously compensated regions. This leaves an iterative design process for multiple targeted frequencies. Ultimately, this makes the time-varying rotor condition challenging to implement.

3.3 Experimental Results

In the experiments presented, the plug-in resonator is used to reject sinusoidal disturbances on the MBC 500 Turbo. Steady-state and time-varying rotor speed conditions are examined as well as controller design configurations.

3.3.1 Control during Constant Rotor Velocity

To examine convergence behavior of the plug-in controllers, the rotor was first spun up to the desired speed (200Hz) under feedback control only, allowed to reach steady-state and the resonator was connected. In the time trace of Figure 3.9, the connection occurs at $t = 20s$ and the resulting transient performance can be observed.

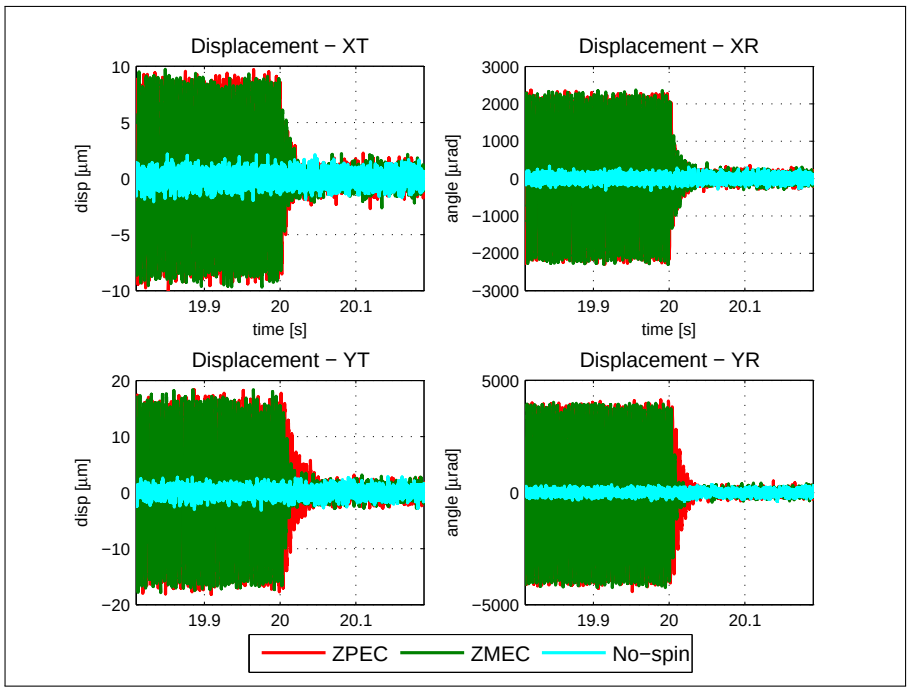

Figure 3.9: Rotor Disp. - Plug-In Resonator Connected at $t = 20s$

Disturbance rejection occurs quickly as the displacements of the four systems reach their steady state value in less than $0.1s$ in all four axes. Both ZPEC and ZMEC inversion methods are implemented and compared. The X-plane systems produce identical results since these methods yield the same inversion filter. In the Y-plane systems, the narrower sensitivity notches of ZPEC in Figure 3.8 reduces the convergence rate compared to ZMEC. In Table 3.1, these values are organized.

Settling Time	XT Δt[s]	XR Δt[s]	YT Δt[s]	YT Δt[s]
ZPEC	0.02	0.03	0.05	0.04
ZMEC	0.02	0.02	0.02	0.02

Table 3.1: Convergence Time - Plug-in Resonator using ZPEC and ZMEC

The RMS of the displacement are organized in Table 3.2. The displacements are shown in the decoupled transformed coordinates. The translational systems are measured in microns while the rotational systems are in micro-radians. Compared to the results under LQGi control only, inclusion of the plug-in resonator with both ZPEC and ZMEC inversion techniques show large reductions indicating the rotor is spinning tighter about its geometric axis and appropriate rejection is taking place. Since $\beta = 1$ in both peak filter designs, the steady-state performance is identical.

Two additional rotor conditions are included. With the LQGi loop closed, the rotor is regulated at the center of the stator. Without any angular velocity, 'Levitate Only' represents a best-case in terms of disturbance rejection. For completeness, the 'Sensor Noise' is also provided to quantify the noise floor of the system. No control action is applied and the rotor is resting against the stator. After removing the bias from this signal, the resulting RMS provides a baseline reading.

Both 1-peak plug-in resonators nearly achieve the ideal rejection mark. The radial vibration in rotor unbalance primarily consists of the primary harmonic at the rotor speed. Designing the filter to target this frequency yields the most performance gains. Though additional performance can gained by designing more peaks in the internal model, the diminishing returns on effort can also be considered. Higher harmonics do exist and their contributions can be better visualized by observing the spectral analysis in Figure 3.10.

When only LQGi is used to stabilize the rotor, the largest spectral component is clearly the shaft speed of 200Hz. The plug-in controllers achieve complete rejection at the designed frequency. The components at the higher harmonics of the rotor speed remain unchanged as no peaks were designed there for these experiments. The remaining spectral disturbances are not amplified beyond what is produced by the LQGi feedback controller.

	LQGi (200Hz)	ZPEC (200Hz)	ZMEC (200Hz)	Levitate Only	Sensor Noise
XT [μm]	5.71	0.66	0.65	0.59	0.57
XR [μrad]	1509.6	95.09	95.21	88.25	85.55
YT [μm]	11.20	0.98	1.01	0.84	0.75
YR [μrad]	2770.3	121.31	124.44	111.76	103.01

Table 3.2: RMS of Displacement - Plug-in Resonator using ZPEC and ZMEC

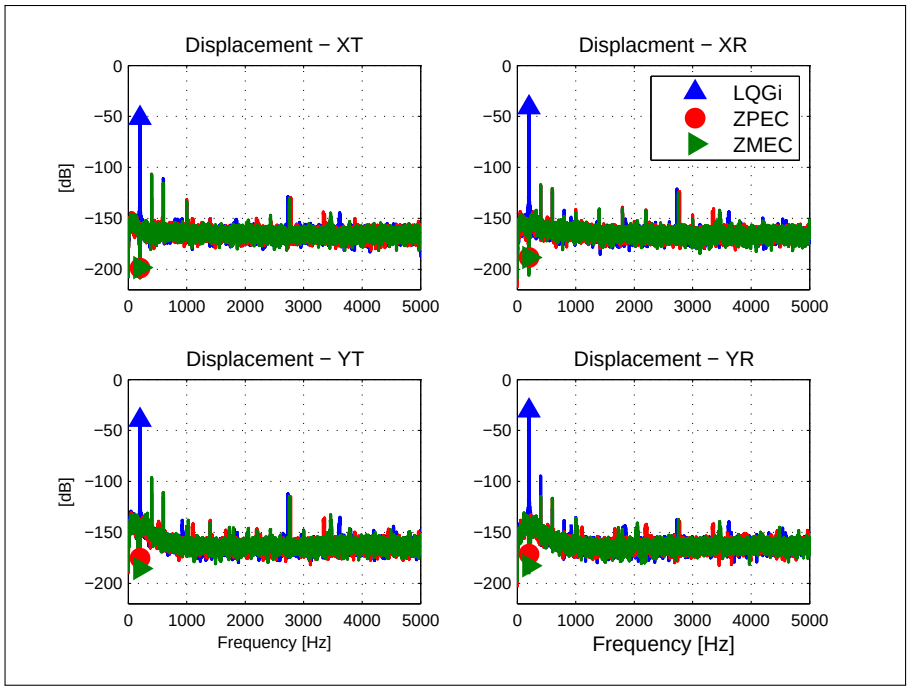

Figure 3.10: Spectrum - Plug-In Resonator using ZPEC and ZMEC

3.3.2 Control during Time-Varying Rotor Velocity

In these experiments, the plug-in resonator for disturbance rejection is examined under time-varying rotor speeds. The velocity profile in Figure 3.11 was specified, though achieving this trajectory is less important than measuring the actual instantaneous velocity of the rotor and placing the peaks at the correct frequencies. The encoder measurement updates the peak filter frequency to place the internal model at the correct position which generates control commands at the first three harmonics of the rotor speed.

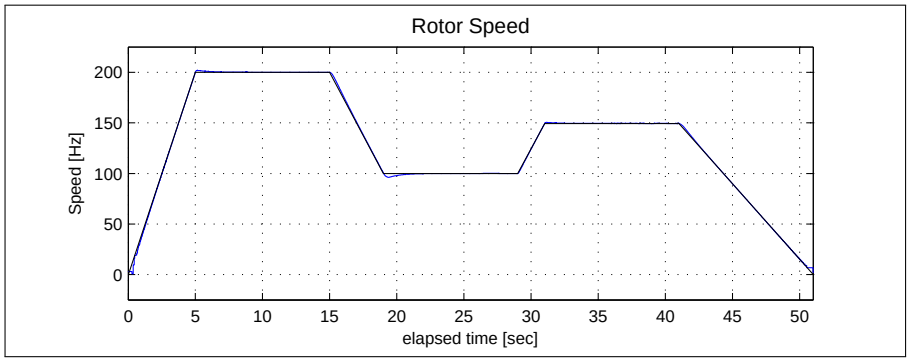

Figure 3.11: General Rotor Speed Profile

From examining the initial PSD in Figure 3.10, the 2^{nd} and 3^{rd} harmonics of the rotor speed also contribute to the disturbance and are natural extensions of the controller. The ZPEC inversion is used to ensure phase compensation over the rotor speed range. The gain γ can be scheduled easily according to the measured rotor speed and provides some stability against the high magnitude of ZPEC. Though ZMEC would produce an ideal magnitude response, the phase compensation aspect made implementation for multiple peaks/time-varying rotor speed difficult.

This profile represents a general velocity change in rotor systems between various set points. The profile was selected to emphasize the various capabilities of the plug-in harmonic resonator. The velocity set points are specified to 200Hz,

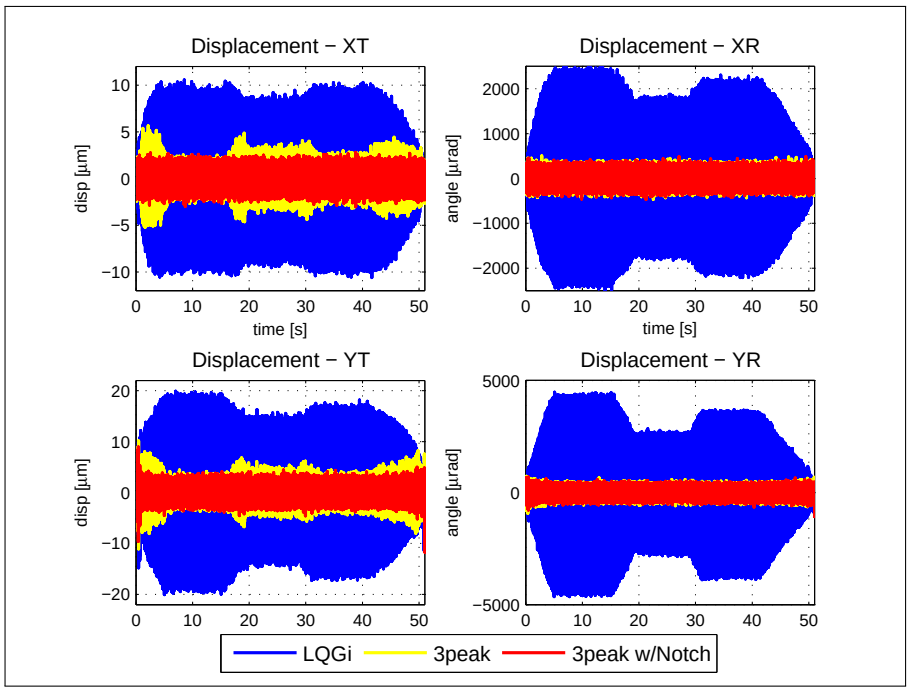

Figure 3.12: Rotor Disp. - 3-Peak Plug-in Resonator for Varying Speed

100Hz and 149.4Hz to demonstrate the flexibility of disturbance rejection. The rates of acceleration and deceleration are also selected with similar intent.

The plug-in resonator is connected throughout the entire run to reduce runout at all rotor speeds. Figure 3.12 compares the measured displacements with and without the plug-in controllers. Additionally, the inversion methods for ZPEC with and without the notch filter are implemented. The plug-in controllers are successful in reducing the large amplitude displacements in all channels. However, there is a loss of performance in the Translational systems when using the standard ZPEC formulation. This is explained by the resonant mode excitation alluded to from Section 2.2. When utilizing the control notch, consistent disturbance rejection is achieved. The RMS of the displacements are compared in Table 3.3 over the entire run.

Figure 3.13 shows the PSD during $36s \leq t \leq 41s$ corresponding to a rotor speed of 149.4Hz. This section was chosen to demonstrate performance when the

		LQGi	3-peak	3-peak w/ Notch	Levitate Only
XT	[μm]	5.23	1.17	0.60	0.59
XR	[μrad]	1231.6	97.27	95.05	88.25
YT	[μm]	9.60	1.60	0.97	0.84
YR	[μrad]	2182.4	135.57	129.75	111.76

Table 3.3: RMS of Displacement - 3-peak Plug-in for Varying Speed

disturbance period is not integer valued nor a multiple of the sample period. Note the excitation of the 2.4kHz mode in the translational systems when using the 3-peak controller. The fact that LQGi does not excite this mode indicates this is a controller excitation and not an exogenous disturbance. An additional peak in the internal model would prove unsuccessful. The 3-peak w/Notch controller addresses this issue and the 2.4kHz component remains at LQGi levels.

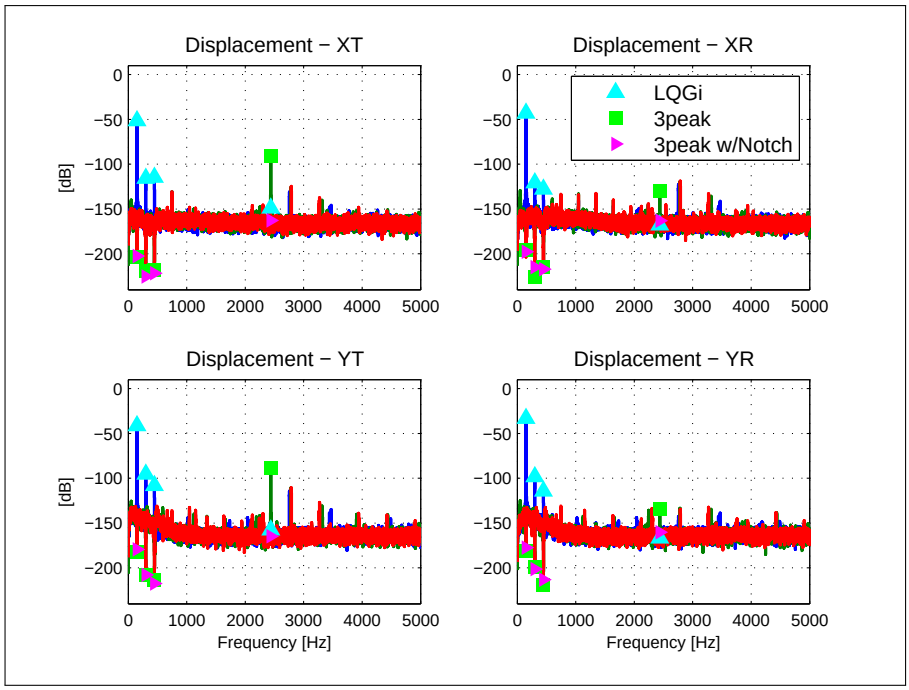

Figure 3.13: Spectrum - 3-Peak Plug-in Resonator at $36 \leq t \leq 41s$

3.4 Summary

In this chapter a plug-in resonator based on the Internal Model Principle was applied to reject harmonic disturbances in an AMB-rotor system. The peak filters of the controller can be designed to reduce any number of frequencies at any location. The frequencies can easily be updated making this controller attractive for time-varying disturbance periods. A stability argument motivated the need for a model inversion filter. Furthermore, system properties required approximate inversion techniques to handle the non-minimum phase zeros of the model. Two traditional approaches were examined. Results presented show superior rejection over feedback control.

CHAPTER 4

Plug-in Repetitive Control

4.1 Introduction

In Chapter 3, a plug-in resonator was presented and implemented on an AMB-rotor system. An approximate model inversion was necessary to satisfy a stability condition. It was noted that due to the nature of the approximations in the methods presented, there were additional filter design considerations.

In this chapter, a more accurate inversion method is explored to improve rejection performance. It will be shown that the main cost of this inversion method is in the number of preview steps required. A better structure to provide this requirement is another plug-in internal model principle type controller, repetitive control. To further improve performance of repetitive control, the peak filter will be incorporated into the design. Experimental results on the system will be presented.

4.2 Direct Inversion of Non-minimum Phase Zeros

The Zero Phase Error Controller (ZPEC) inversion is a classic approach to invert non-minimum phase systems due to the benefits of phase inversion. However, with unstable zeroes close to the unit circle, the magnitude response can be quite high in high frequency. An FIR approximate inversion of the non-minimum phase zeros, referred to as Direct Inversion (DI), was implemented in [CT14].

Using the same factorization as (3.9), the Direct Inversion filter is defined as

$$F_{DI}(z^{-1}) = \frac{A(z^{-1})}{z^{-d}B^{+}(z^{-1})} \cdot B_{DI} \tag{4.1}$$

which inverts the stable portion and approximates the unstable zero inversion by

$$\begin{aligned} \frac{1}{B^{-}} &= \left[\frac{1}{[B^{-}]^{*}}\right]^{*} && (4.2)\\ &\approx \left[\frac{1}{[B^{-}]^{*}}\right]^{*}\Bigg|_{N_{DI}} && (4.3)\\ &= B_{DI} \end{aligned}$$

where the * denotes conjugation of the filter. The direct inversion of the unstable zero produces an unstable IIR (4.2). The conjugate filter is stable (poles reflected inside the unit circle). Conjugation is also equivalent to a reflection of the impulse response across $t = 0$ in the time-domain. This produces a non-causal stable filter with infinite impulse response. The IIR can be approximated sufficiently with an N_{DI} number of taps which require N_{DI} preview steps for causality (4.3).

As a measure of accuracy of the inversion method, the product with the plant model is shown in Figure 4.1. Compared to the previously utilized ZPEC, the DI method yields a vastly more accurate magnitude response for the two non-minimum phase systems. Recall, the X-plane systems are minimum phase and thus can be fully inverted without approximation.

The cost of the DI filter is in the increased amount of preview steps required, given by $m = d + N_{DI}$ for the system delay d and the filter order N_{DI}. Compared to the ZPEC requirement of $d + n_u$, where n_u is the number of unstable zeros, this preview cost will be substantially higher. In the plug-in resonator formulation, the preview step requirement was provided by lifting the peak filter to generate an m-order internal model. As the lifting requirement gets larger, the internal model become cumbersome and susceptible to numerical issues as the $m-1$ aliased peaks begin to crowd the spectrum.

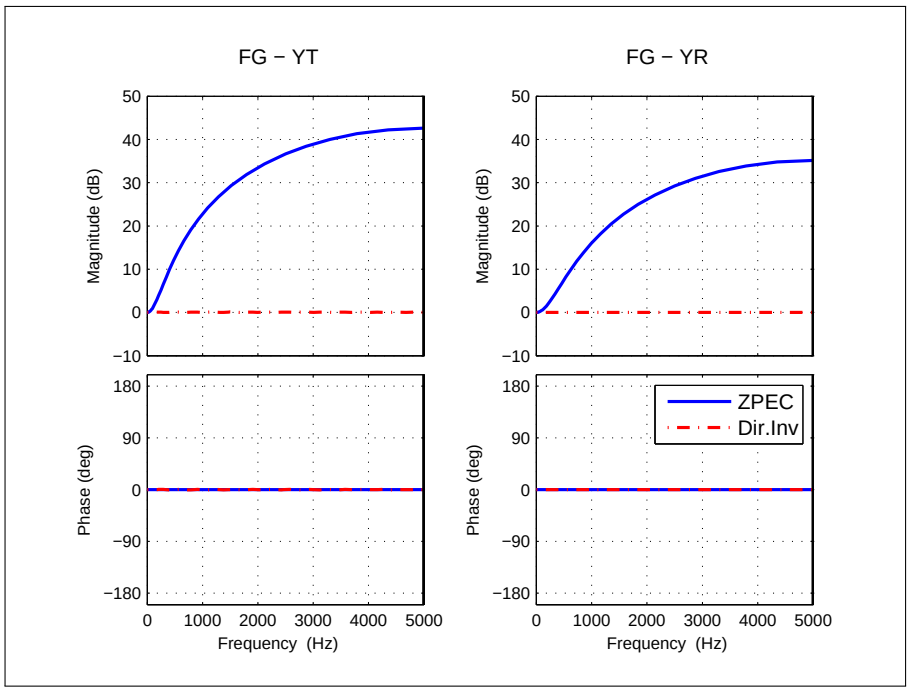

Figure 4.1: Comparison of Plant Inversion Methods

4.3 Plug-in Repetitive Control

To make use of this more accurate inversion method, incorporation into the plug-in repetitive control structure is proposed. The Prototype Repetitive Controller (PRC) [TTC89] exhibits many of the same useful properties in stability and performance as the plug-in resonator. Similarly, the repetitive controller is connected as a plug-in module to a pre-closed feedback loop in Figure 4.2.

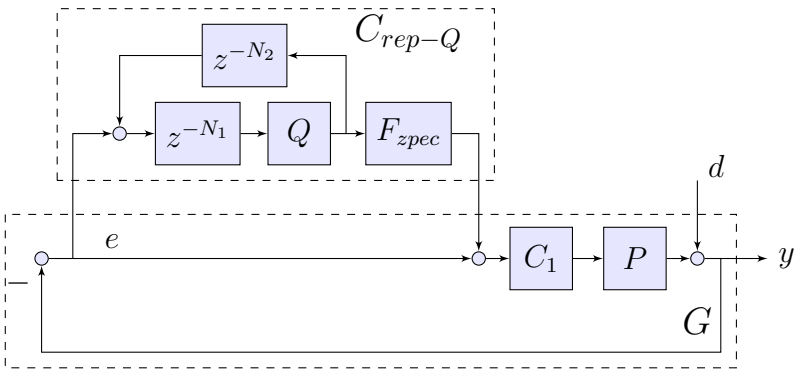

Figure 4.2: Block Diagram of Prototype Repetitive Controller

The internal model is generated by wrapping a positive feedback loop around an integer delay block. The delay length $N_p = \frac{1/T_s}{\omega}$ represents the disturbance period in multiples of the sample time. This generates infinite control action at primary disturbance period, as well as all integer multiples up to the Nyquist frequency. Control generated at these higher harmonics can destabilize the system. To provide robustness, a zero-phase low-pass filter

$$Q(z, z^{-1}) = (.25z + .5 + .25z^{-1})^{n_q} \tag{4.4}$$

is typically included to attenuate control signals past the cutoff frequency where the order n_q of the filter adjusts the cutoff. The symmetric coefficients determine the sharpness of the corner in Q and can similarly be used to design the appropriate filter. The delays in Figure 4.2 are then given by $N_1 = N_p - m - n_q$ and $N_2 = m$ where m is the required preview steps to emulate depending on the inversion filter method.

The benefits of the DI filter are first examined in the PRC formulation. Figure 4.3 compares the repetitive controller gains

$$C_{r,Q} = \frac{Qz^{-N_p}}{1 - Qz^{-N_p}} \tag{4.5}$$

where the low pass filter Q is designed to primarily satisfy the robust stability criterion in the closed-loop system.

Though the positive delay feedback generates many harmonics of the primary disturbance period, depending on the conservativeness of the low-pass filter, these harmonics are attenuated. In primarily satisfying the robust stability criteria, the magnitude amplification of the ZPEC inversion requires Q to be quite conservative and essentially attenuate all signals except the primary harmonic. The DI inversion method produces a more favorable magnitude inversion and thus allows the Q-filter order to be relaxed. The cutoff frequency is higher and more harmonics are generated. Allowing the controller to generate more harmonics at

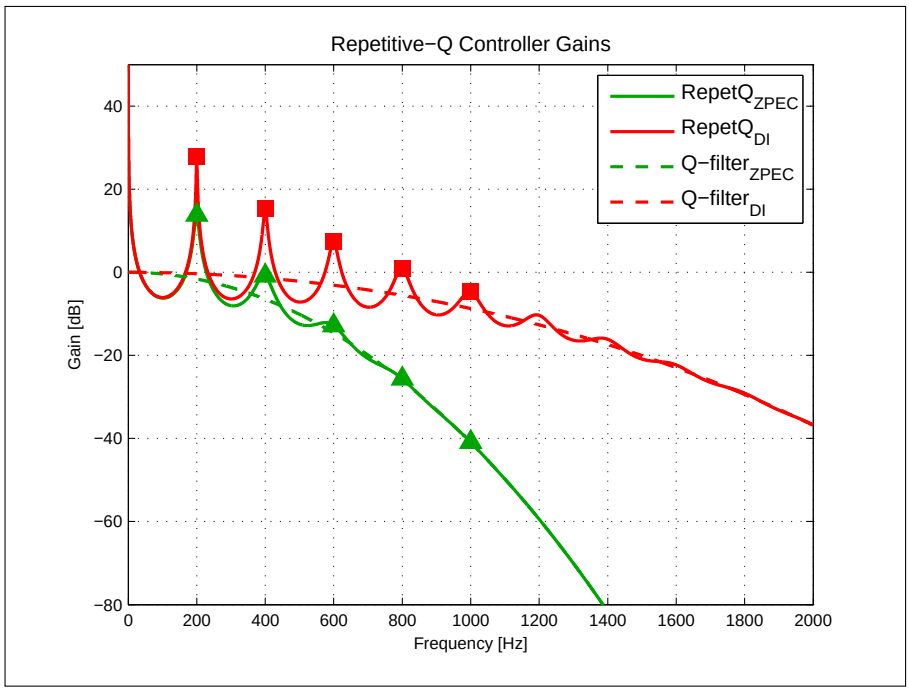

Figure 4.3: Repetitive Controller Gains using Different Inversion Methods

higher amplitudes will positively effect the convergence and steady-state rejection performance when using the DI algorithm.

4.3.1 Repetitive Control with Peak Filter

Yet, the use of the low-pass filter for robustness presents some shortcomings. From Figure 4.3, even in the pass-band of Q, the expected infinite gains at the harmonics of 200Hz are attenuated. Because the cutoff of Q is not ideal, the pass-band gain is close to but not exactly unity. Stability must strictly be enforced, yet no additional parameter other than the order of Q is available for design. The bandwidth of each peak nor the gains are easily tuned but are at the mercy of the design of Q. In short, the quality of the controller peaks cannot be directly governed. To address this, higher-order repetitive control can be used to shape the controller [Ste02, PDD08].

The block diagram in Figure 4.4 is proposed to take advantage of both the

more accurate Direct Inversion method as well as to use peak filters in place of the low pass filter.

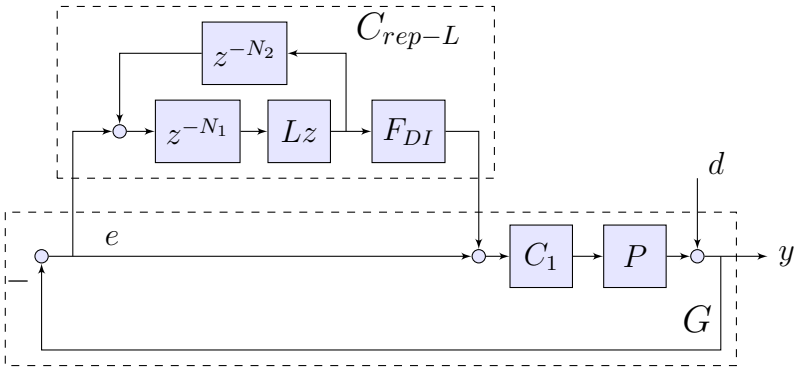

Figure 4.4: Block Diagram of Plug-In Repetitive Controller with Peak Filter

These peak filters were generated by first designing a series of 2^{nd}-order notch filters and inverting them.

$$H = \prod_{k=1}^{p} \frac{1 - 2\beta_k \cos\omega_k z^{-1} + \beta_k^2 z^{-2}}{1 - 2\rho_k \cos\omega_k z^{-1} + \rho_k^2 z^{-2}} \tag{4.6}$$

$$L = 1 - H \tag{4.7}$$

Filter L is an attractive alternative to Q in that it is 0 mostly everywhere, serving the same purpose as Q to eliminate unwanted high-frequency harmonic control components.

$$L(z^{-1}) = \begin{cases} L = 1 \text{ if } \omega = \omega_{k=1,2,\ldots p} \\ L \approx 0 \text{ if } \omega \neq \omega_k \end{cases} \tag{4.8}$$

In other words, the feedback loop will generate the infinite gain integer harmonic control effort and the designed peak filters turns the relevant harmonics on and off. An added benefit of this filter design is to reduce the inter-harmonic amplification common to PRC. The Bode sensitivity integral states that a reduction in closed-loop sensitivity in some band, must be balanced by an equal amplification in

another band. This so-called "Waterbed Effect" in PRC is a significant factor since the notches generated are numerous and wide.

Design of parameters β and ρ provides direct control over the shape and quality of the notches (and eventual peaks). β can be interpreted as the aggressiveness of the notch. $\beta = 1$ will place the zeros on the unit circle resulting in infinite gains. It can also be tuned to satisfy stability conditions on the closed-loop system. $\rho < \beta$ maintains the correct shape of the filter while their relative relationship

$$BW_{Hz} \approx \frac{\pi(1-\rho_k)}{2\pi T_s} \tag{4.9}$$

can be used to determine the -3dB bandwidth of each notch. The bandwidth of each peak provides direct design over the robustness to uncertainty in frequency. Thus, the number of harmonics, the aggressiveness (gain) and the bandwidth of the control peak can all be designed independently to preserve stability of the system while enhancing performance.

Figure 4.5 compares a set of L parameters and their subsequent control gains. A set of narrower but taller peaks is useful when the disturbance frequency remains constant. Narrower peaks will disturb the stability less while the taller peaks allow higher control gains. Another shorter yet wider set is more forgiving of frequency mismatches, useful in varying or uncertain rotor speed conditions. Note that even within each set, each peak can be designed independently providing the designer more freedom to make appropriate choices given the makeup of their disturbance.

For the disturbances in the MBC 500 Turbo, it was determined that five harmonics of the rotor speed are significant thus the filters were designed to include only those that were relevant. Higher harmonics were also found to contribute less. In one set, the first three harmonics have infinite gains while the 4^{th} and 5^{th} harmonics are reduced to prevent unnecessary inter-harmonic amplification. When the rotor speed is constant, these aggressive parameters can be used for better

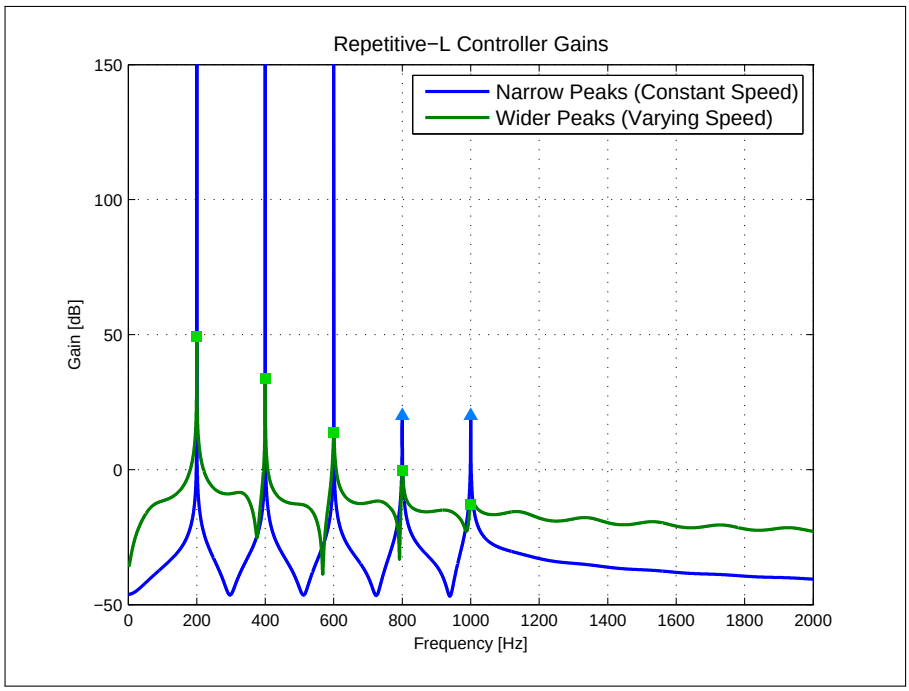

Figure 4.5: Repetitive-L Controller Gains - Different Peak Filter Parameters

rejection. For cases near stability conditions or if the rotor is changing speeds, the controller can be designed to be more forgiving. These gains are reduced to allow the peaks to be wider and absorb more uncertainty in the disturbance frequency.

4.3.2 Stability and Sensitivity Analysis

The robust stability analysis is similar to that presented in Chapter 3 and thus only the results are presented here. The complimentary sensitivity function can be found from (3.19) and the stability condition verified.

In Figures 4.6 and 4.7, the robust stability criterion is investigated for the repetitive controllers designed. For comparison, the results of LQGi are also included. The three versions of repetitive control are presented; RepetQ-ZPEC, RepetQ-DI, and RepetL-DI. Firstly, it is clear that all formulations are robustly stable. Using this robust stability condition as the primary design tool, the filters were allowed to be as aggressive as possible without violating this condition.

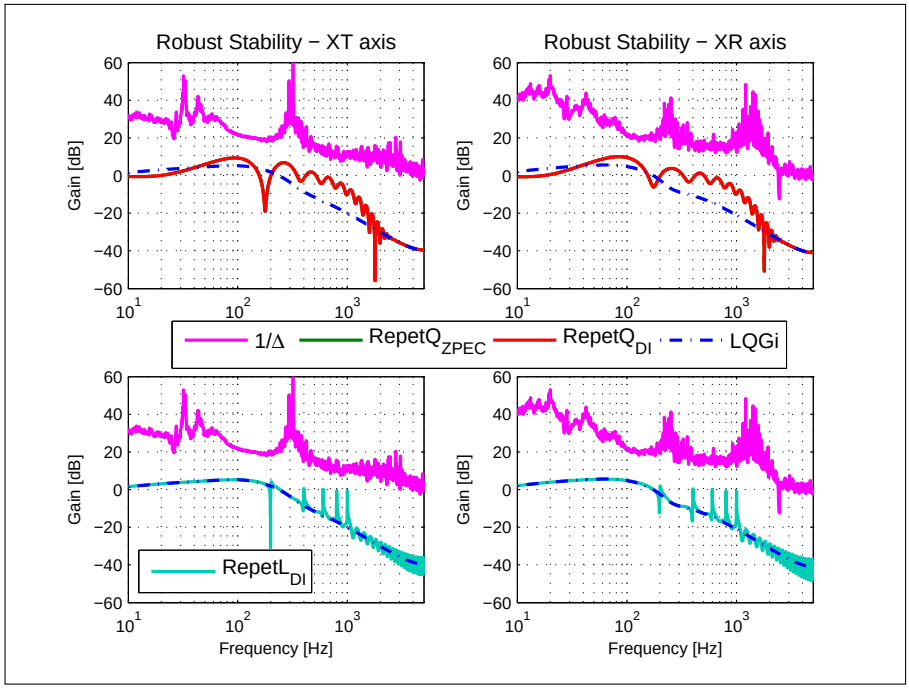

Figure 4.6: Robust Stability of Plug-In Repetitive Controllers - X-axis

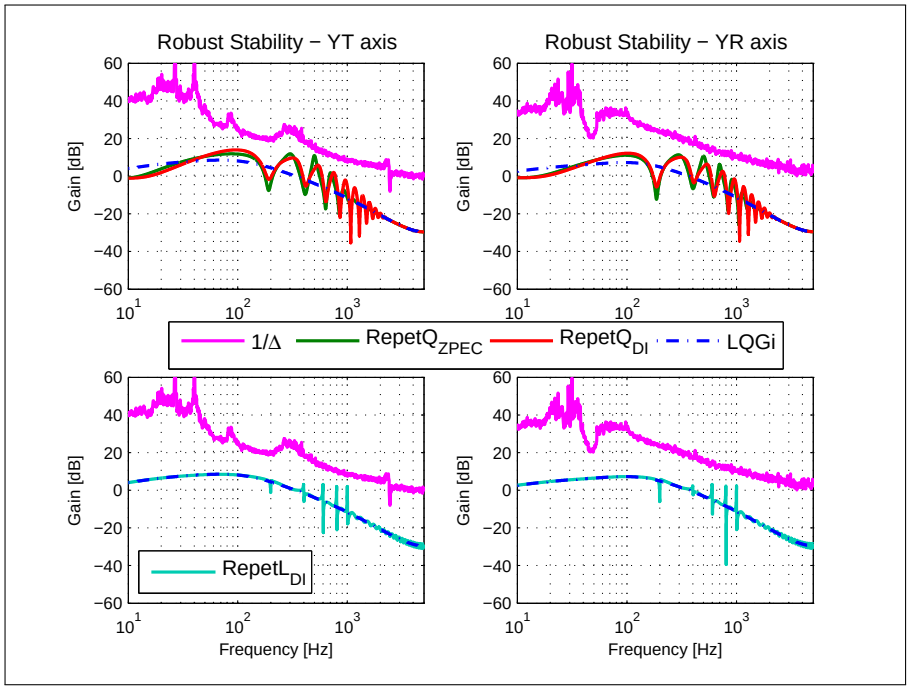

Figure 4.7: Robust Stability of Plug-In Repetitive Controllers - Y-axis

In the X-plane systems in Figure 4.6, both Q-filter methods produce the same result and thus their results overlap. The RepetL-DI disturbs the stability of the closed-loop system less and only narrow peaks are generated. In the Y-plane systems in Figure 4.7, the results are similar. We note the tight margins in the RepetQ methods. The amplifications in the pass-band of Q requires conservative design which effect the expected performance seen in the sensitivity analysis.

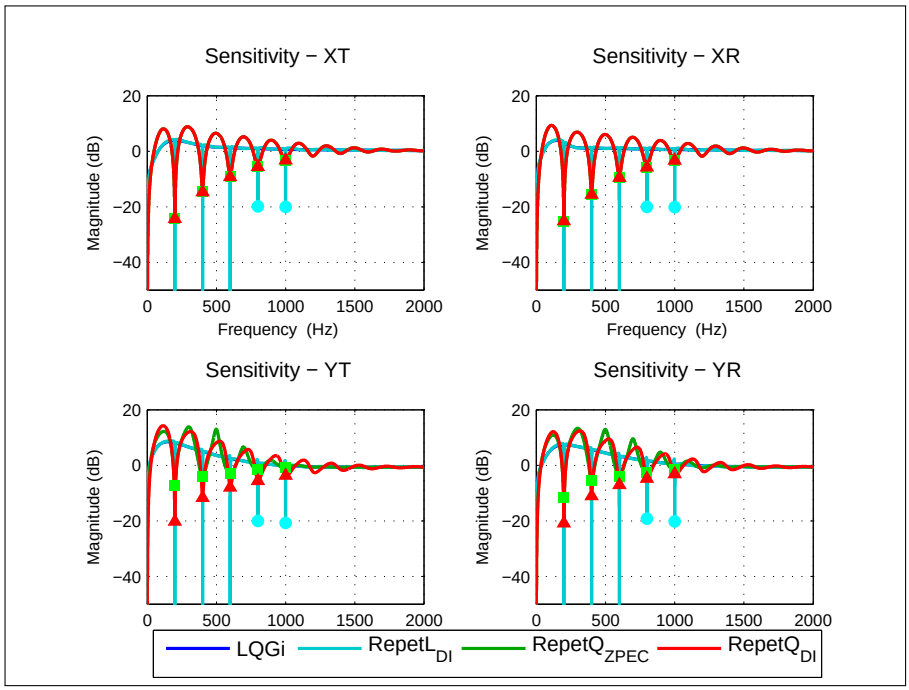

Figure 4.8: Sensitivity Analysis of Plug-In Repetitive Controllers

The closed-loop sensitivity functions of (3.20) are examined in Figure 4.8. The decrease in controller gains by the Q-filter results in a reduction in sensitivity to disturbances at the harmonic frequencies. Also evident are the regions of inter-harmonic amplification that occurs in both Repet-Q formulations. Any performance gains made by reducing the disturbances could be diminished by the increase in signal components in these amplified bands. The use of the L improves both the aggressiveness of the harmonics as well as reduces the Waterbed Effect.

4.3.3 Fractional Delay Filter

The internal model in repetitive control is generated by integer delays. In practical rotor-bearing applications, the rotor speed is a continuous spectrum and will often be a non-integer multiple of the sample time. Mismatches between the integer delay lengths and the true disturbance period cause loss in rejection performance [THD07]. For these time-varying cases, the delay lengths must be updated on-line to provide proper compensation. One approach calculates the desired delay length and rounds to the nearest integer [TQN98]. Of course, the problem remains that when the disturbance period is between integer values, performance will suffer. Some researchers have made use of fractional delay filters which approximate the non-integer portion of the delay as an FIR filter in order to capture inter-sample behavior [YH00, WWZ07].

The Lagrange interpolator provides a simple implementation method since the filter coefficients can be given in closed-form [LVK96]. Linear interpolation was found to provide adequate response in the AMB-rotor operating range.

The required delay can be calculated from

$$\begin{aligned} N_p &= \frac{{}^{1}/_{T_s}}{\omega} \\ &= \lfloor N_p \rfloor + d \end{aligned} \tag{4.10}$$

where the integer delay is used to update the integer delay block the non-integer portion is used in the linear interpolation fractional delay FIR filter given by

$$X = (1 - d) + dz^{-1} \tag{4.11}$$

4.4 Experimental Results

In the experimental results presented, the designed controllers were applied to the AMB-rotor system to reject the sinusoidal disturbance caused by rotor unbalance. Both constant and time-varying rotor speed conditions are presented.

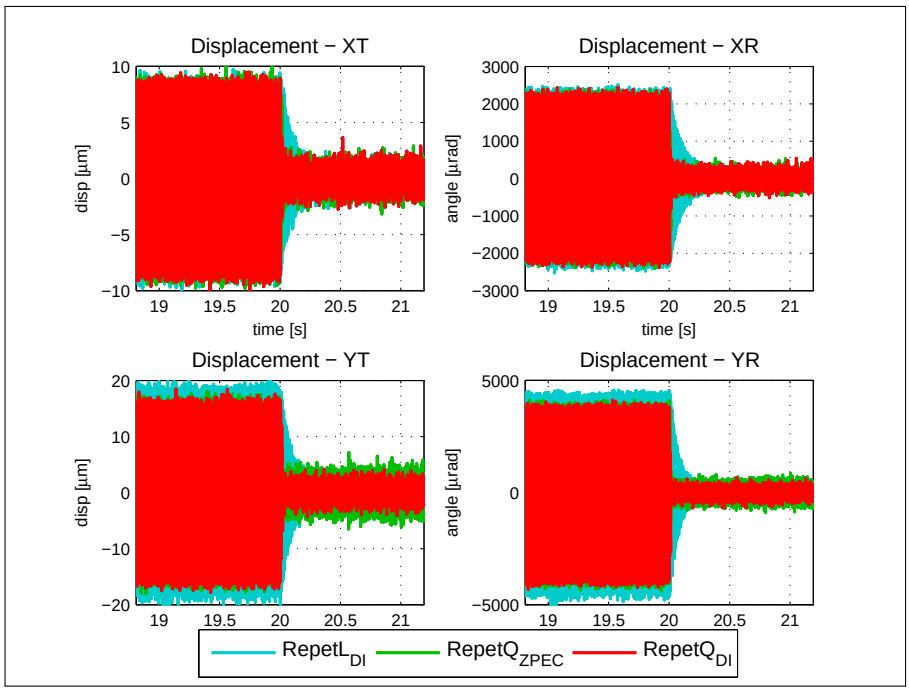

Figure 4.9: Rotor Disp. - Repetitive Control Connected at $t = 20s$

4.4.1 Control during Constant Rotor Velocity

In the time trace of Figure 4.9, the rotor is spun to a desired speed (200Hz) under feedback control only. The repetitive controller is connected at $t = 20s$ and the resulting transient performance can be observed. Disturbance rejection occurs quickly as the displacements of the four systems reach their steady state value in less than $0.1s$ in all four axes.

Both Q-filter formulations converge much faster than Repet-L, also seen in Table 4.1. This is due to the width of each peak generated in the controllers shown in Figures 4.3 and 4.5. The peaks of Repet-L are designed to be much more narrow to improve steady-state rejection performance of these controllers. The L-filter is designed to generate much higher control authority at the interested frequencies while simultaneously reducing inter-harmonic amplification.

Steady-state rejection performance is quantified through the RMS error in Table 4.2. The displacements are shown in the decoupled transformed coordinates.

Settling Time	XT Δt[s]	XR Δt[s]	YT Δt[s]	YT Δt[s]
Repet-Q-ZPEC	0.02	0.02	0.01	0.02
Repet-Q-DI	0.01	0.02	0.03	0.02
Repet-L-DI	0.25	0.31	0.25	0.23

Table 4.1: Convergence Time - Plug-in Repetitive Controllers

	LQGi only	Repet-Q ZPEC	Repet-Q Dir.Inv	Repet-L Dir.Inv	Levitate Only
XT [μm]	5.71	0.75	0.74	0.61	0.59
XR [μrad]	1509.6	139.13	136.52	95.65	88.25
YT [μm]	11.20	2.18	1.19	0.90	0.84
YR [μrad]	2770.3	289.10	168.83	132.49	111.76

Table 4.2: RMS of Displacement - Plug-In Repetitive Controllers

The translational systems are measured in microns while the rotational systems are in micro-radians. Column 'LQGi' represents the stable levitation of the rotor during constant rotational velocity when only LQGi is used. The RMS is clearly larger due to the strong disturbance caused by rotor unbalance. Implementing the plug-in repetitive controllers show large reductions indicating the rotor is spinning tighter about its geometric axis and appropriate rejection is taking place. Since $\beta = 1$ in the L-filter design, there is increased rejection performance. Even between the two Q-filter methods, using the Direct Inversion method allows the low-pass filter to be less restrictive and thus enjoys better performance as well. An additional rotor condition measurements is included for comparison. Without any angular velocity, 'Levitate Only' represents a best-case in terms of disturbance rejection.

Spectral analysis over this same interval is compared in Figure 4.10. When only the LQGi controller is used, the main disturbances represent the unbalance due to rotor unbalance and the first four overtones. In the X-plane systems, both Q-filter methods yield the same performance since both inversions will yield the same filter. Using the peak filter increases the rejection performance and completely removes the disturbance to the noise floor.

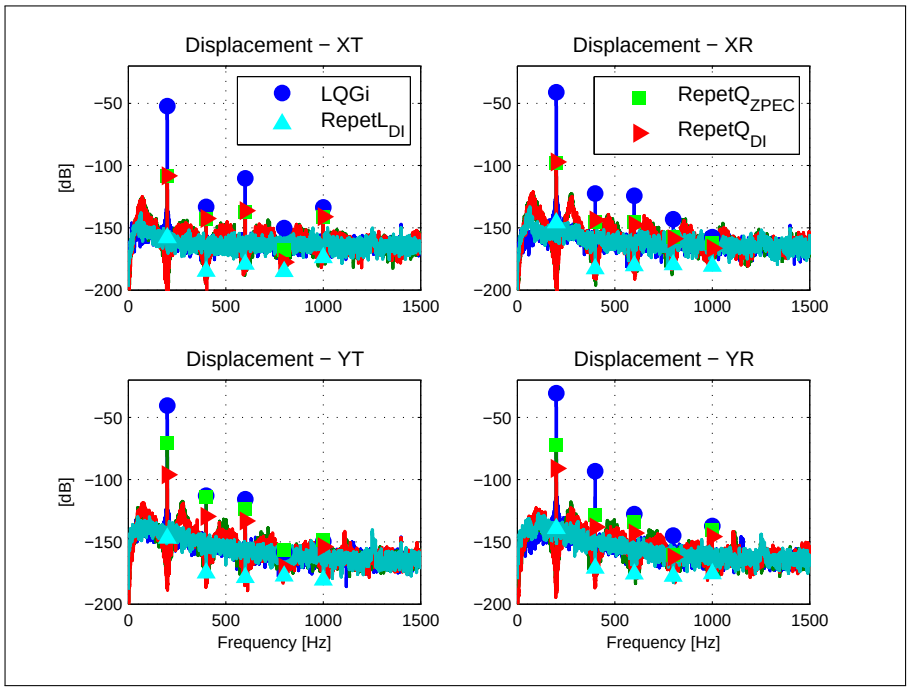

Figure 4.10: Spectrum - Plug-In Repetitive Controllers

In the Y-plane systems, the consequences of each controller strategy is more apparent. The DI filter allows the Q-filter to be less restrictive, thus removing more of the disturbances through the spectrum. Yet, both Repet-Q methods suffer from inter-harmonic amplification as indicated by the ripples in the spectral analysis. Using both L and DI filters produce the best results in both narrowly removing the disturbances without amplifying any unwanted bands.

4.4.2 Control during Time-Varying Rotor Velocity

These control strategies can be further examined under time-varying rotor speed conditions. The speed trajectory in Figure 4.11 was applied to the system for each of the repetitive control versions. The plug-in controllers are active during the entire duration and the delay lengths adapted using the encoder measurement of the system.

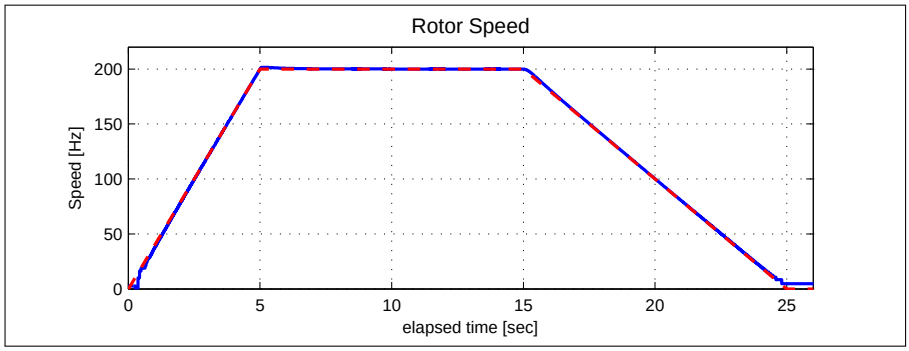

Figure 4.11: Applied Rotor Speed Profile

The Repet-Q controllers are unchanged as they were designed at the limit of the stability bounds. Considering L-filter design, if the bandwidth of each peak is not sufficiently wide, the controller will not be robust to mismatches in rotor speed. Taking advantage of the design freedoms provided by the peak filter formulation, a more forgiving parameter set can be determined.

In the rotor speed profile applied in Figure 4.11, the displacements in the speed up-to-constant speed region is highlighted in Figure 4.12. The two parameter sets of the L-filter are switched at $t = 5$s when the rotor speed transitions from ramping to constant. A simple first-order rate limiter on the parameters reduces any instability caused by a sudden change in control signal.

Compared to LQGi only, all repetitive controllers are capable of tracking the rotor speed and reducing the runout effects. As expected, Repet-L outperforms the other two methods over the course of the entire run. The RMS of these

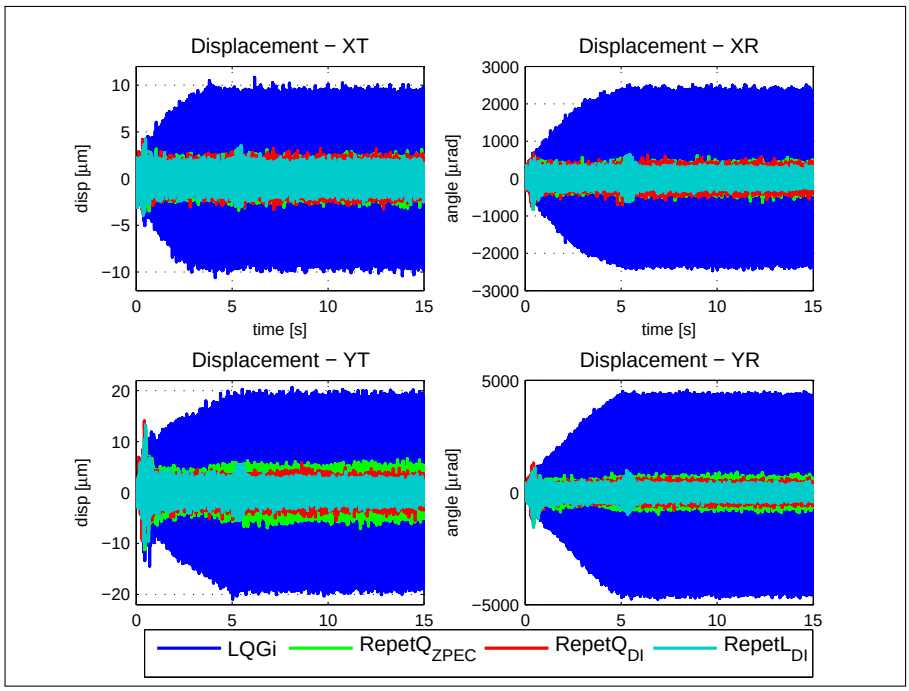

Figure 4.12: Rotor Disp. - Ramp-up Region ($0 \leq t \leq 15$) of Figure 4.11

displacements are organized again in Table 4.3.

	LQGi only	Repet-Q ZPEC	Repet-Q Dir.Inv	Repet-L Dir.Inv
XT [μm]	5.29	0.74	0.74	0.66
XR [μrad]	1387.3	137.99	137.4	112.25
YT [μm]	11.09	2.07	1.36	1.16
YR [μrad]	2668.2	270.82	186.11	162.83

Table 4.3: RMS of Displacement - Time-Varying Speed

4.5 Summary

In this chapter a plug-in repetitive controller with peak filter and direct inversion filter was presented and implemented on an AMB-rotor system. This was

compared against a more typical repetitive control strategy as well as the Q-filter with direct inversion method. The inclusion of repetitive control shows marked improvement in reducing the effects of rotor unbalance when compared to stabilizing feedback controller only. Due to the superior design freedoms and more direct control over controller properties, Repet-L provides more disturbance rejection over the two Repet-Q methods in both constant and time-varying speed conditions.

CHAPTER 5

Multivariable Plug-in Resonator

5.1 Introduction

The underlying approach in the previous chapters was based on a decoupling assumption which allowed for single-input single-output (SISO) design and analysis. Given that the AMB-rotor system is naturally a multi-input multi-output (MIMO) system, a more accurate model based on the coupled coordinate is examined.

In this chapter, the higher order coupled models of the system are used to perform multivariable control design. A periodic trajectory will be applied to the rotor ends while the disturbance due to rotor unbalance is minimized. A multivariable version of the plug-in resonator will implemented. The plant inversion used previously to satisfy a stability condition will be accomplished through a simple method. The controller will be implemented on the system and results presented.

5.2 Modeling

In Chapter 2, system ID data collected was manipulated using a geometric argument to produce four decoupled SISO plant models representing the translation and rotational of the rotor in the X and Y-planes. This was done to simplify the design and analysis process. To regulate each rotor end within the center of the AMB, it is also possible to control the system in the original coordinate system.

Using the same collected data, the inter-planar decoupling assumption is removed and higher order 2x2 multivariable models are developed. Figures 5.1 to 5.4 show the results of the multivariable model fit onto the X-plane and Y-plane data. The resonance mode is captured in these models as well as the cross-channel behavior.

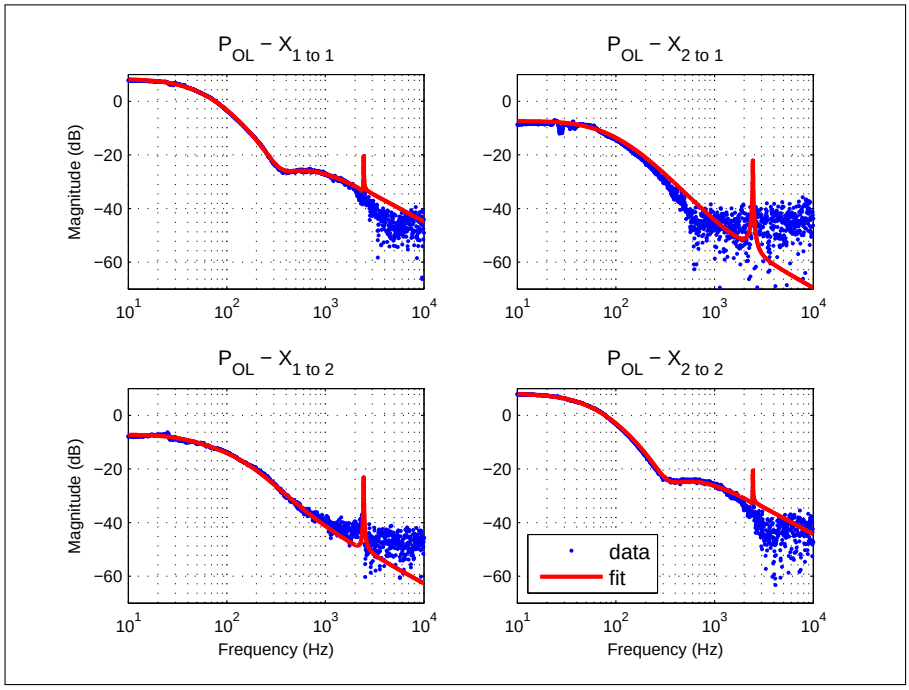

Figure 5.1: Model Fit of X-Plane Raw Coordinates (Magnitude)

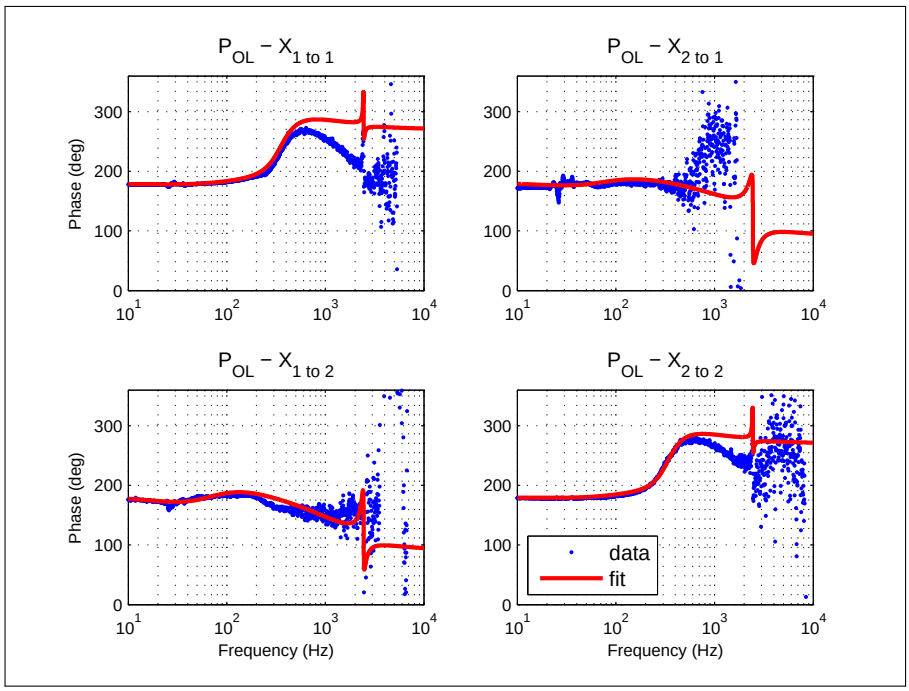

Figure 5.2: Model Fit of X-Plane Raw Coordinates (Phase)

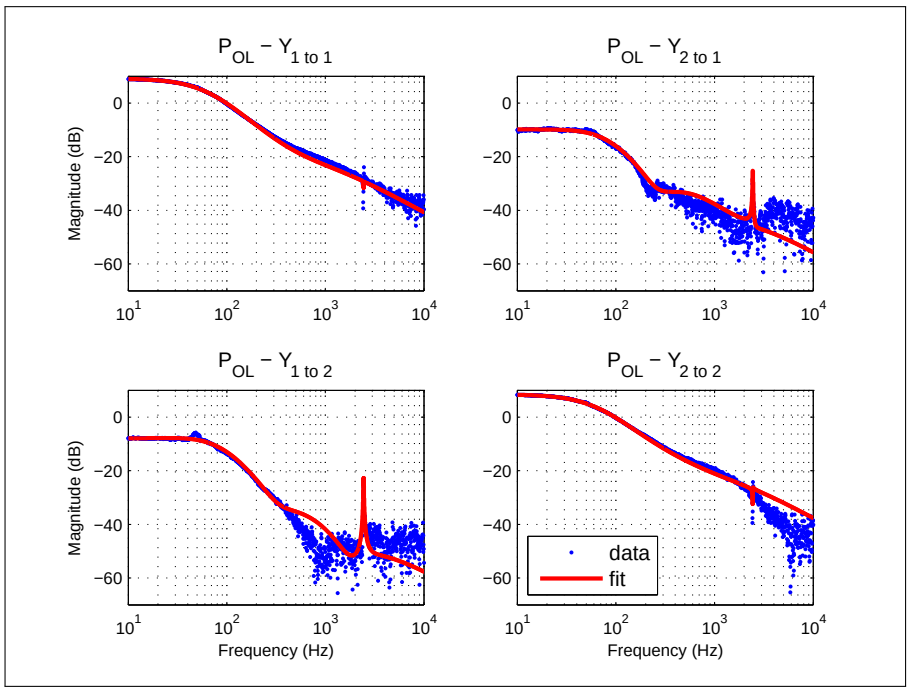

Figure 5.3: Model Fit of Y-Plane Raw Coordinates (Magnitude)

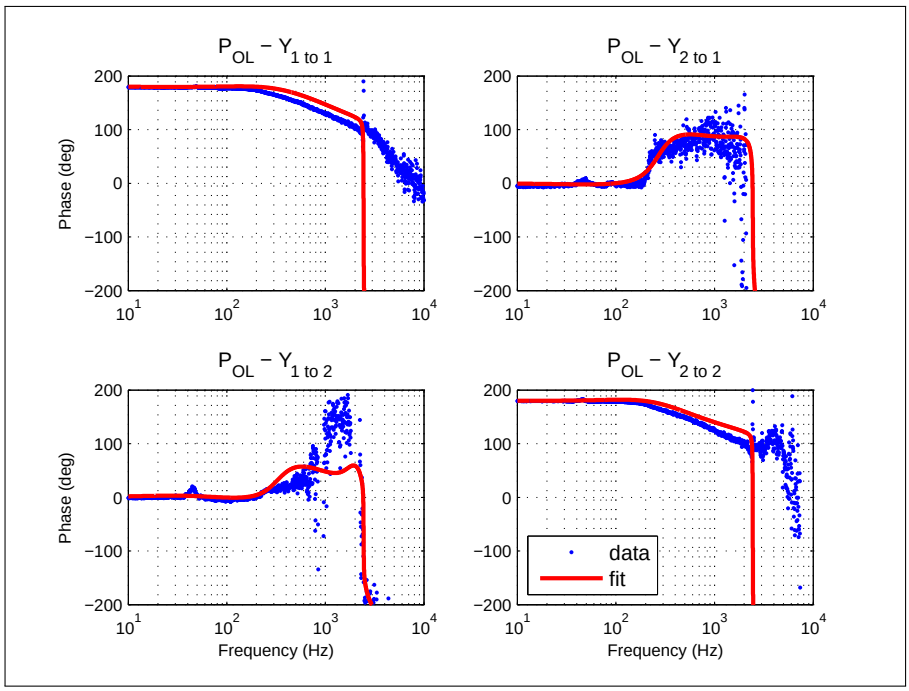

Figure 5.4: Model Fit of Y-Plane Raw Coordinates (Phase)

Many of the SISO model properties apply to the MIMO systems: the open-loop requires a robust stabilizing controller and the Y-plane system also contain unstable zeros. Following the same procedure, a multivariable LQGi feedback controller was used to stabilize the system.

5.3 Multivariable Plug-in Resonator

The plug-in harmonic resonator can be easily generalized as a MIMO formulation. As a plug-in to the pre-stabilized system G, the block diagram can be reorganized into Figure 5.5.

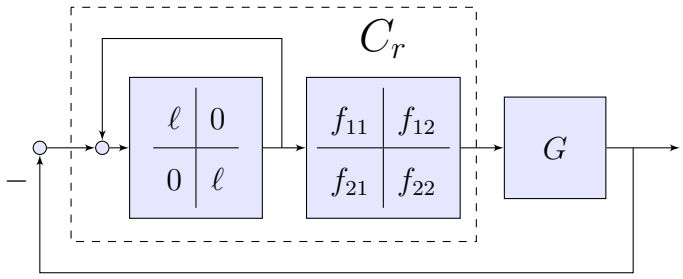

Figure 5.5: Components of Harmonic Resonator in MIMO

Discussion of the design of the internal model and peak filters from Chapter 3 are directly applicable and will be omitted here in the interest of brevity.

5.3.1 Discrete Approximate Inversion for Stability

The motivation for the F filter still applies from the conservative Nyquist stability argument of (3.7). Rewritten in matrix notation as

$$\|L(I - FG))\|_\infty < 1 \tag{5.1}$$

where the internal model filter L here is a diagonal transfer function matrix where ℓ are the SISO inverted notch filters. The MIMO peak filter easily satisfies (5.1) by design, and the stability criterion can be reduced to a similar filter design problem

$$\|I - FG\|_\infty < 1 \tag{5.2}$$

In the SISO approach, this was satisfied through plant inversion methods like ZPEC. In the multivariable case, these methods become complex to apply. Thus, a more simple and straightforward approach of finding a filter such that

$$F(e^{j\omega_i}) = G^{-1}(e^{j\omega_i}) \tag{5.3}$$

is applied since it is only necessary at those $e^{j\omega_i}$.

For the $w(k)$ frequencies the peak filter is designed at, the plant model can be evaluated to generate complex matrices. A matrix inversion will provide then

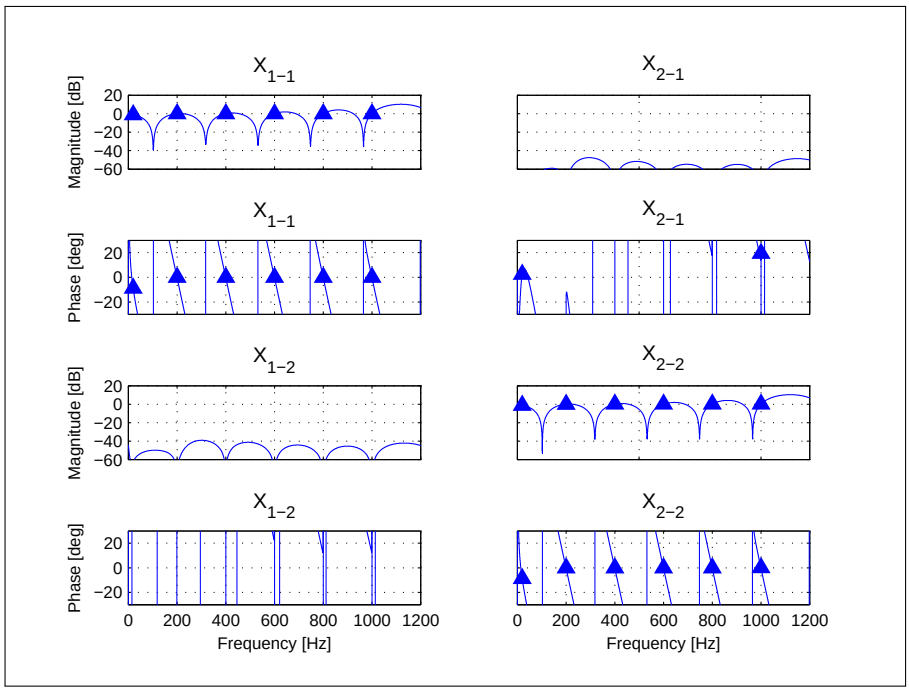

Figure 5.6: Discrete Point Multivariable Inversion for X-plane Model

produce the $g(k)$ set of of complex "coordinates" the inversion filter must pass through. This simply becomes a filter design problem for each of the f_{mn} shown in Figure 5.5. The search is conducted over FIR filters to produce a stable inversion where the identified filter coefficients will minimize a weighted sum of the fit error between the data g and filter B

$$\min_{b} \sum_{k=1}^{n} wt(k)\|g(k) - B(w(k))\|^2 \tag{5.4}$$

The weighting vector $wt(k)$ is an additional design tool to allow tolerance in the fit to produce well-behaved filters over the spectrum.

The accuracy of the discrete point-wise inversion is seen in Figures 5.6 and 5.7 to satisfy (5.3) within tolerance. At the prescribed frequencies, the magnitude response is approximately the identity matrix. The peak filter in the internal model is designed to track a 20Hz sinusoidal profile while rejecting the rotor unbalance at 200Hz and a few of its harmonics.

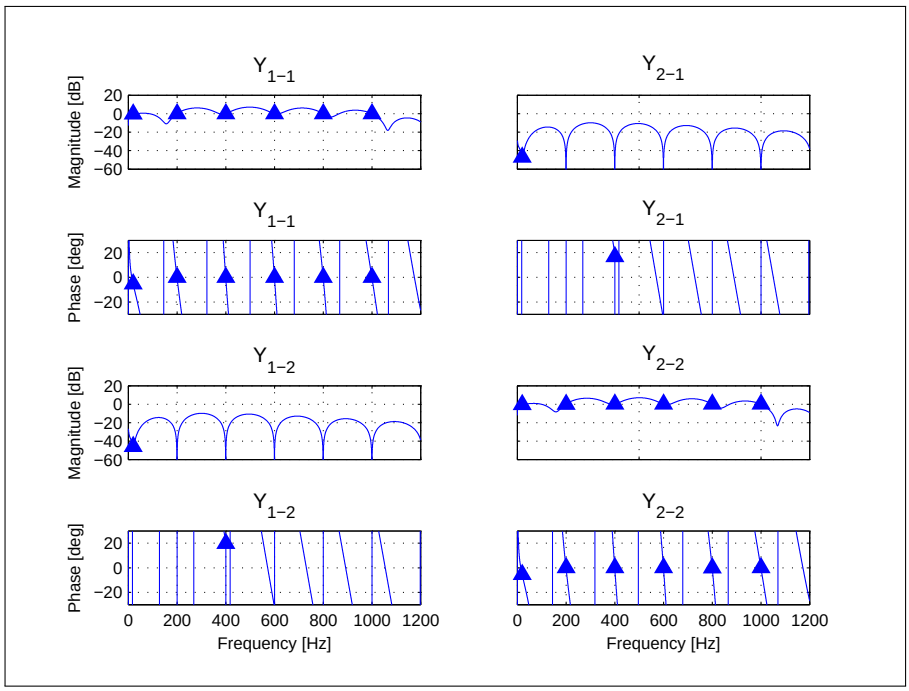

Figure 5.7: Discrete Point Multivariable Inversion for Y-plane Model

5.4 Experimental Results

The results presented demonstrate the efficacy of the multivariable approach in tracking a sinusoidal profile in each of the rotor endpoints while simultaneously rejecting the radial vibration due to rotor unbalance. The same conditions are applied for a SISO design on the MBC 500 Turbo and the results are compared.

5.4.1 Control during Constant Rotor Velocity

The rotor was spun up to the desired speed (200Hz) before the reference trajectory was applied. The trajectory applied to each rotor end is a sinusoid with amplitude 20μm. The X-coordinate and Y-coordinate are $\frac{pi}{2}$ radians out of phase. This produces the circular trajectory of diameter 40μm.

The improvements in tracking performance for both rotor ends is evident in the time traces shown in Figure 5.8. Under LQGi control, the MIMO controller

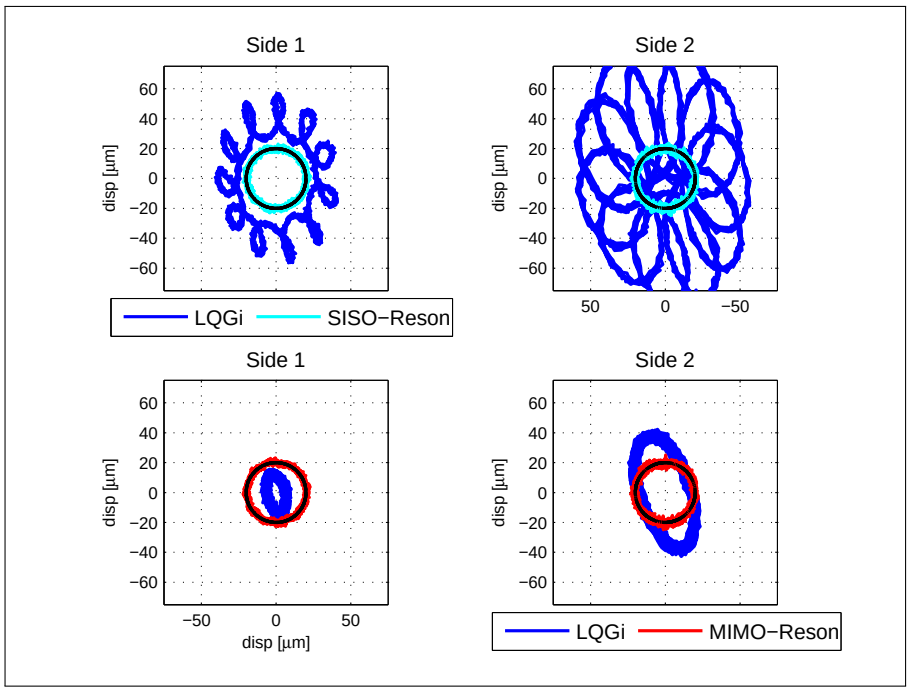

Figure 5.8: Rotor Disp. - Rotor-End View in Steady-State

outperforms the SISO version. This is most likely attributed to the coordinate transformation performed in the decoupling process. Recall that the SISO systems are interested in the geometric center of the rotor. The reference signal also undergoes the same coordinate transformation, and by this metric, the geometric centers appear well regulated. However, this allows the rotor ends to traverse a more exaggerated trajectory. Once the resonator is connected, even in the SISO case, the disturbance and tracking error are driven down.

The RMS of the error is organized in Table 5.1 and show the improvement indicated by the time traces. In both approaches, the incorporation of the resonator drives the error down to equivalent levels.

The spectrum of the error signal is also analyzed in Figures 5.9 and 5.10. The plug-in resonator eliminates error due to both tracking and disturbances. The MIMO version maintains all the stability and sensitivity benefits the SISO formulation has. The spectrum is narrowly effected with minimal amplification

RMS Error	X1 [μm]	Y1 [μm]	X2 [μm]	Y2 [μm]
SISO-LQGi	19.32	18.52	10.58	34.96
MIMO-LQGi	14.99	17.02	20.03	30.00
SISO-Reson	0.97	1.13	0.90	1.42
MIMO-Reson	0.89	1.13	0.97	1.44

Table 5.1: RMS of Error - Plug-in Resonator SISO vs. MIMO

in the other bands.

Because the inversion applied here is inherently discrete, it would be difficult to operate when the rotor speed is changing. The stability condition would not be satisfied for the other frequencies. Further work would be required to make it applicable for time-varying rotor speed cases.

5.5 Summary

In this chapter, the plug-in resonator was extended to the multivariable case. Much of the derivation was similar including the benefits of the peak filter satisfying the sufficient stability condition most everywhere. The model inversion was performed using the strict interpretation of the stability condition which only requires the inversion to hold at discrete points. An FIR filter was used to interpolate the resulting inverted points. A profile tracking component was included in the experiments to illustrate the benefits of designing the controller in the coupled domain.

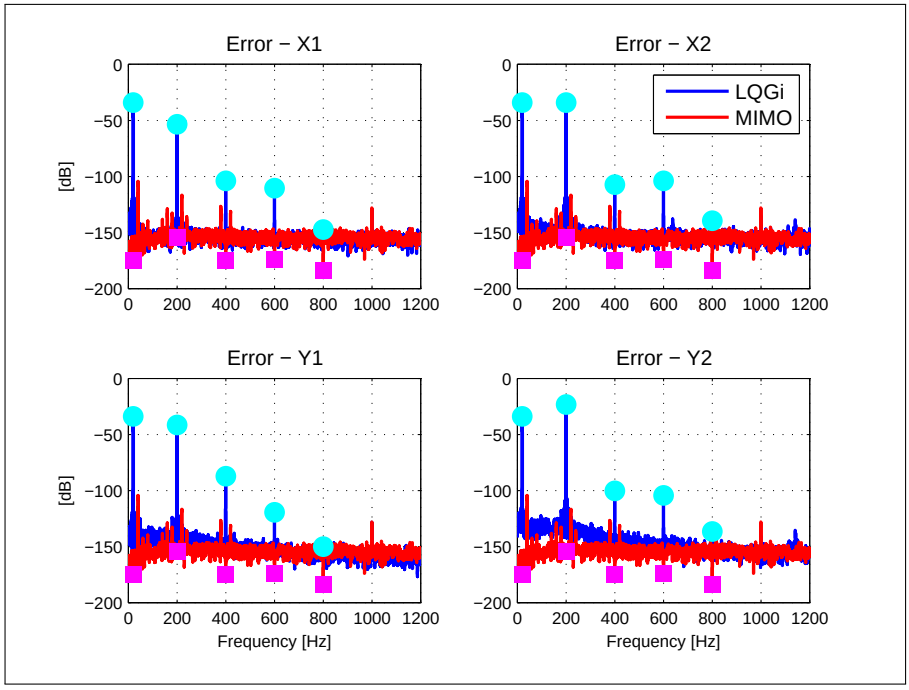

Figure 5.9: Spectrum - MIMO Plug-in Resonator

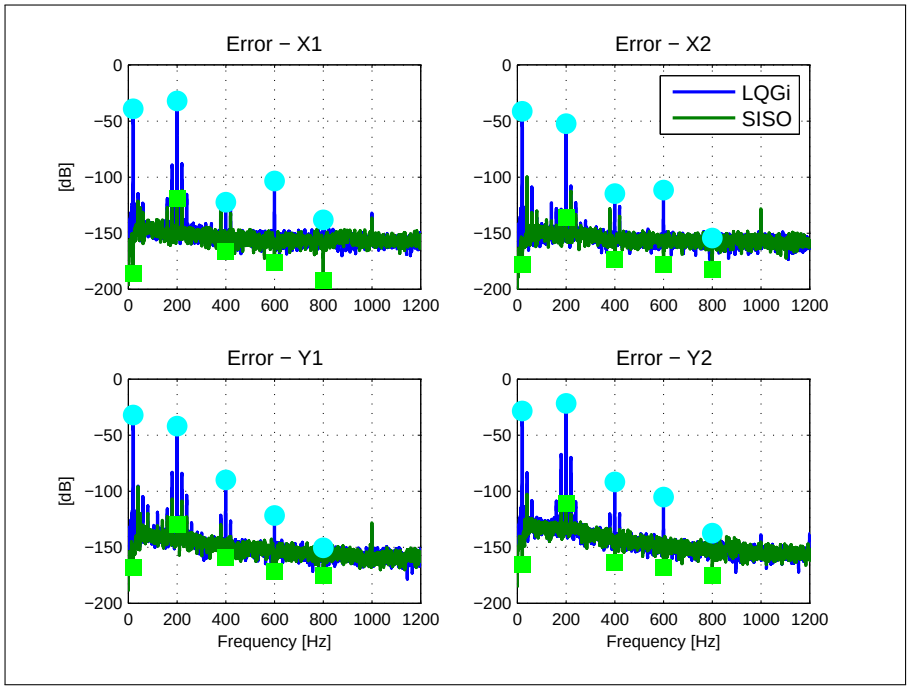

Figure 5.10: Spectrum - SISO Plug-in Resonator

CHAPTER 6

Plug-In Resonator with Adaptive Filter for Complex Disturbances

6.1 Introduction

In the work presented thus far, the disturbance has been sinusoidal stemming from rotor unbalance. The plug-in resonator and repetitive control strategies have been well-suited for disturbances of this type. However, if the disturbance were more complex in nature and contained broadband elements, the internal model approach would no longer be effective. This chapter presents some collaborative work with Nolan Tsuchiya, from the Beam Control Laboratory at UCLA, aimed at rejecting complex disturbances on the AMB-rotor system.

Aside from the disturbance characterization, the remaining design considerations remain unchanged. Stability remains of critical importance. In a dual control strategy, a receding-horizon adaptive controller is designed for broadband disturbance rejection [TGV13,TGT13]. The peak resonator is utilized as a plug-in module to this loop. This chapter will describe the control structure and present experimental results on the system.

6.2 Control Design

The disturbances can be separated into a sinusoidal component and a broadband sequence. The harmonic components are a result of rotor unbalance, which gen-

erates disturbances at the rotor speed and a few of its harmonics. The broadband noise is produced through a shaker installed under the AMB-rotor system.

The Resonator and Receding-Horizon controllers are implemented in the block diagram structure shown in Figure 6.1. This configuration allows the pre-stabilized closed-loop system, $G = \frac{PC_1}{1+PC_1}$ to remain relatively undisturbed. The feedback controller C_1 (e.g. LQG with integral action) is used to stabilize the system while the additional controllers enhance the performance in a narrow capacity.

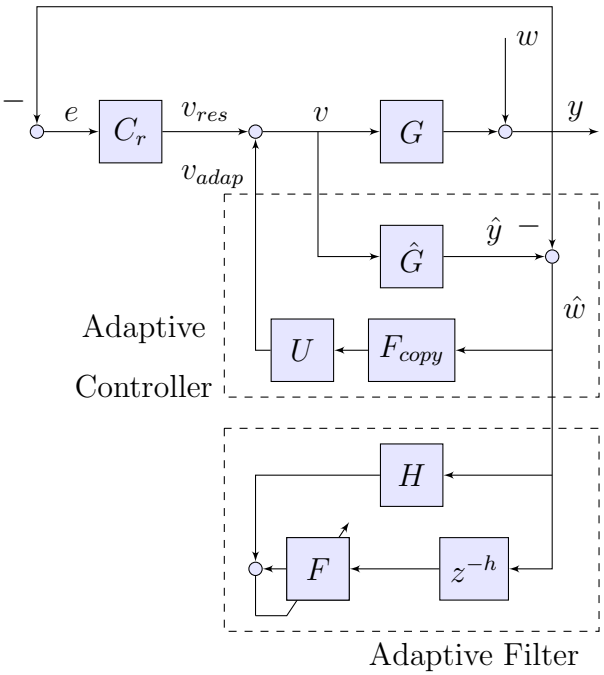

Figure 6.1: Block Diagram of Resonator and Adaptive Controllers Structure

For an accurate plant model ($\hat{G} = G$), it can be shown from Figure 6.1 that the equivalent transfer function the resonator sees will reduce to $\hat{G}$. This makes designing the plug-in resonator independent of the adaptive filter. Furthermore, $\hat{G} = G$ also implies that $\hat{w} = w$ and thus the adaptive filter also can be designed independently of the internal model controller.

$$e = -\frac{1}{1 + C_r\hat{G}} \cdot (1 + UF\hat{G})w \tag{6.1}$$

This result makes this structure quite attractive in rejecting complex disturbances with both deterministic and stochastic components. The resonator can be designed to eliminate the harmonic components while maintaining stability of the closed-loop system. Simultaneously, the adaptive controller can focus on the broadband disturbances to improve the performance over any one controller alone.

The plug-in resonator, described in Chapter 3 is implemented and discussion will be omitted here. It was designed to reject the first five harmonics of the rotor speed.

6.2.1 Receding-Horizon Adaptive Control for Broadband Disturbance Rejection

The receding-horizon adaptive controller uses a model of the plant to identify the disturbance and generate a control command by adapting filter F to minimize the variance of the error e due to $\hat{w}$ and subject to the quadratic cost defined as

$$J_h(\hat{x}(t), \hat{w}_h(t), v_h(t)) = \sum_{k=1}^{h} \left[e^T(t+k) Q_1 e(t+k) + \hat{x}^T(t+k) Q_2 \hat{x}(t+k) \right] + \sum_{k=0}^{h-1} \left[u^T(t+k) R_u u(t+k) \right] + \hat{x}^T(t+h) Q_3 \hat{x}(t+h) \tag{6.2}$$

to weight the error, estimates states, and control effort. This cost is taken over a fixed-length horizon h, where the vectors $w_h(t)$ and $v_h(t)$ are predicted disturbances and control commands, respectively, h-steps into the future. The weighting matrix R_u is used penalize control effort in the frequency domain. Essentially, it allows the control authority to be strong in the lower frequencies where most of the disturbances reside. Simultaneously, the higher frequency components of v_{adap} are more heavily penalized, reducing the excitation of high-frequency plant modeling errors and nonlinearities which can degrade performance and cause instability in extreme cases.

The receding-horizon control command is a linear function of the estimated states and estimated disturbance

$$v_{adap}(t) = UF\hat{w}(t) \tag{6.3}$$

$$= -K_x\hat{x}(t) - H_w\hat{w}_h(t) \tag{6.4}$$

which minimizes the performance index, where K_x and H_w are defined in terms of the state-space matrices and the weighting matrices in (6.2).

For closed-loop stability, from Figure 6.1, U must be stable:

$$U(z) = (\hat{A} - \hat{B}K_x, \hat{B}, -K_x, I) \tag{6.5}$$

This can be guaranteed by choosing the weighting matrices in (6.2) such that the resulting gain matrix K_x makes $\hat{A} - \hat{B}K_x$ stable. One way to guarantee stability of $\hat{A} - \hat{B}K_x$ is to then choose the weighting matrix Q_3 in (6.2) such that

$$\hat{C}^T Q_1 \hat{C} + Q_2 + Q_3 = P \tag{6.6}$$

where the symmetric matrix P is a stabilizing solution to the algebraic Riccati equation associated with the estimated disturbance and (6.2).

6.3 Experimental Results

In the following experimental results, the rotor is spun to 200Hz to generate the harmonic disturbances. The shaker also connected to generate a broadband vibration between 50-100Hz. The results of the experiment are represented by the translational system in the X-plane and the rotational system of the Y-plane. These were chosen as illustrative examples of the full data set and reduce redundant display of results.

To study both transient and steady-state performances, only the feedback controller is used to bring the rotor to the desired speed. At time $t = 20$s,

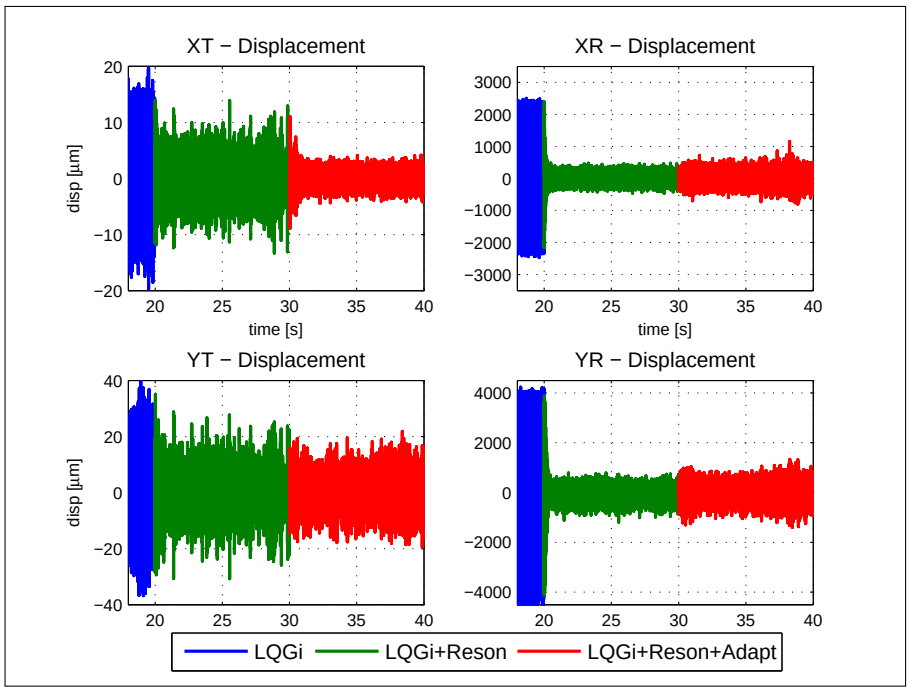

Figure 6.2: Rotor Disp. - Resonator Connected at $t = 20$s and Adaptive Filter Connected at $t = 30$s

the resonator is first connected to eliminate the harmonic components. Then at $t = 30$s, the adaptive filter is connected. The controllers connected in this order allows the adaptive filter to learn mostly the broadband disturbance.

From Figure 6.2, when the resonator is connected, the XT time trace shows a large reduction in amplitude fairly quickly indicating strong rejection. The broadband shaking is also apparent from jagged appearance. When the adaptive filter is connected, no change in the displacement is visible for a short duration while the filter is learning the disturbance. Once it does, it reaches its steady-state levels quickly.

In the YR time trace, the resonator performs as expected by reducing much of the harmonic disturbance. However, the shaker disturbance does not seem to contribute much this axis and when the adaptive filter is connected, there is clear and evident loss in rejection performance. The spectrum of the measured outputs

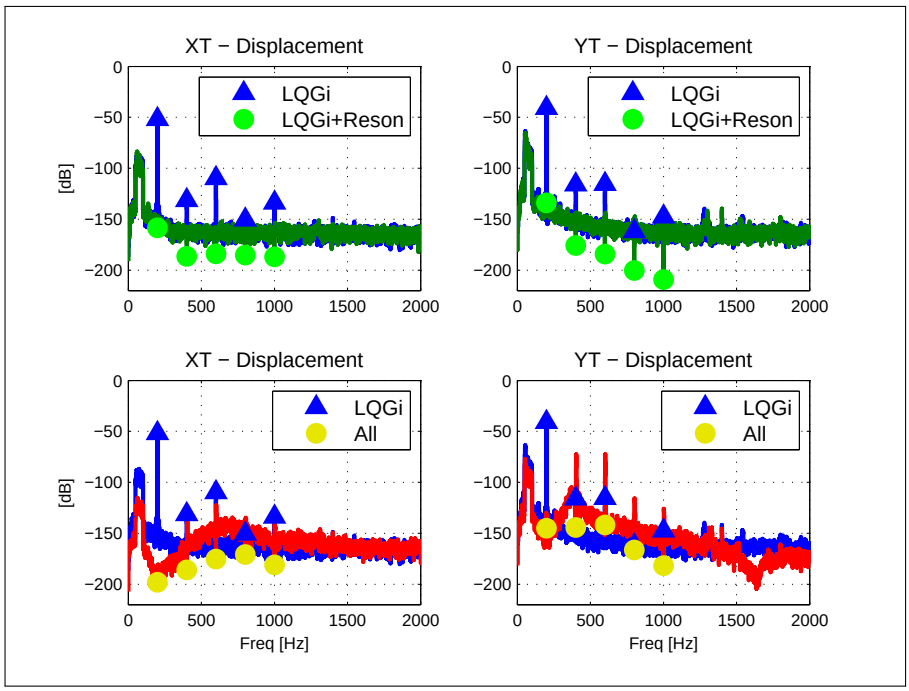

Figure 6.3: Spectrum - Translational Displacement Systems

indicate amplification of the spectrum by the adaptive filter in Figure 6.4.

From Figures 6.3 and 6.4, the disturbances can be seen via the spectrum of the measured output. When under LQGi control only, the rotor remains under stable operation though disturbance rejection is minimal and thus their spectral components are distinctly visible. The Translational systems shown in Figure 6.3, exhibit the full shaker disturbance. When using the resonator only, this band between 50-100Hz is unaffected. Connecting the adaptive filter reduces this disturbance roughly 20dB. In the Rotational systems shown in Figure 6.4, we note that the shaker disturbance do not contribute much. And as indicated by the time trace, once the adaptive filter is connected, portions of the spectrum are amplified above the LQGi output including near the rotor speed harmonics.

The RMS of the output error is tabulated in Table 6.1 for all the four systems. In the XT system, as well as the YT system, the best result is had when both controller are used together to narrowly target each disturbance. In the Rotational

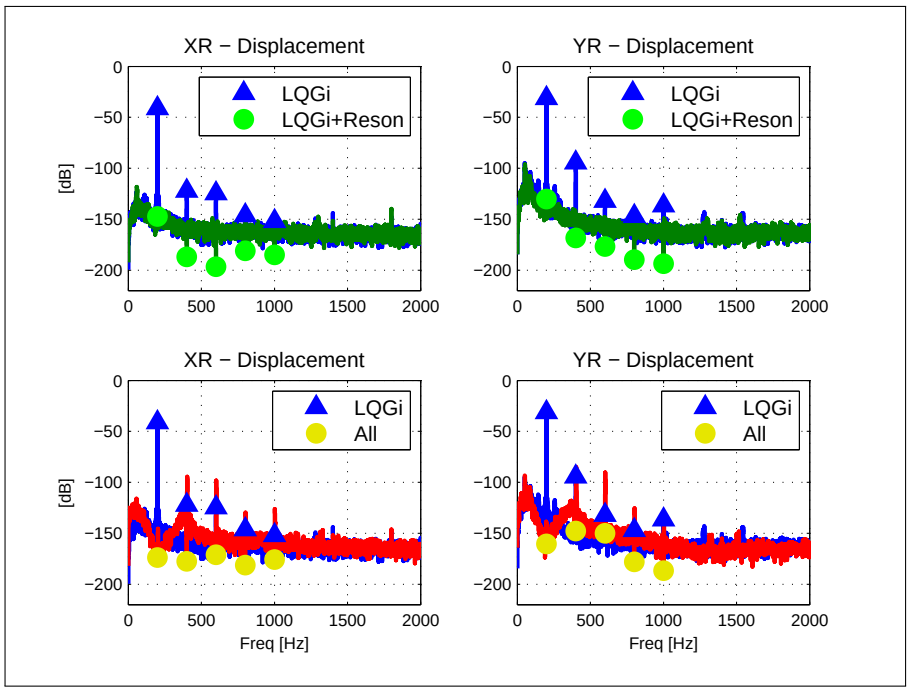

Figure 6.4: Spectrum - Rotational Displacement Systems

systems, the RMS performance when using both controllers is worse than when only the Resonator is used due to the amplification caused by the aggressive adaptive filter. This is most likely due to the over-parameterization of the adaptive filter order for a relatively minimal disturbance.

	LQGi	LQGi+Reson	LQGi+Reson+Adapt
XT [μm]	6.57	3.15	0.97
XR [μrad]	1498.54	108.71	155.68
YT [μm]	13.24	7.26	4.85
YR [μrad]	2679.28	201.06	279.83

Table 6.1: RMS of Displacement - Plug-In Resonator with Adaptive Filter

6.4 Summary

In this chapter the plug-in resonator was combined with a receding-horizon adaptive controller to reject both harmonic and broadband disturbances in an AMB-rotor system. The controllers were applied in a plug-in architecture to minimally effect the stability of the underlying stabilizing controller while also not affecting the other control scheme. Results presented show superior rejection over feedback control, though certain cases showed loss of rejection performance.

CHAPTER 7

Conclusion

This dissertation presented the use of a plug-in resonator for harmonic disturbance rejection on an AMB-rotor system. Due to the specific design consideration, the plug-in resonator is an appropriate candidate for control. The plug-in structure provides robustly stable design and implementation while also increasing the rejection performance of the disturbance. The formulation of the controller motivated a model inversion for stability, which required some approximate inversion techniques due to the non-minimum phase zeros present in a couple of the models. A few traditional approaches were applied.

The shortcomings identified in the traditional approximate inversion methods presented an opportunity to explore other more accurate inversion methods. An FIR approximation of the direct inversion of the unstable zero was found to produce superior inversions. The high non-causal requirement was provided by the repetitive control structure. The standard low-pass filter for robust stability in repetitive control make the controller much too conservative. It was further improved by incorporating the peak filters from the plug-in resonator to produce better rejection performance.

Furthermore, the inter-planar decoupling assumption was removed to extend the plug-in resonator into a MIMO formulation. The more accurate plant model, which accounted for the resonant mode of the system as well as the cross-coupling, was better able to track a profile with the rotor ends while simultaneously rejecting the harmonic disturbances from rotor unbalance.

Lastly, a complex disturbance was rejected using an adaptive filter and the resonator in tandem. The controllers were arranged such that each controller could be designed independently on the pre-stabilized system. A shaker was used to emulate a broadband disturbance. When the complex disturbance existed, the dual controller method showed superior rejection performance. When the shaker did not contribute disturbance, the adaptive filter was over-parameterized and thus amplified other regions of the spectrum which resulted in a loss of performance.

References

[AJE06] Inigo Arredondo, Josu Jugo, and Victor Etxebarria. "Modelling of a Flexible Rotor MagLev System." In *American Control Conference, 2006*, pp. 406–411, June 2006.

[BL00] Mingsian R. Bai and Weibin Luo. "DSP Implementation of an Active Bearing Mount for Rotors Using Hybrid Control." *Journal of vibration and acoustics*, **122**(4):420–428, April 2000.

[BLP99] Patrick Barney, James Laugger, Rebecca Petteys, James Redmond, and William Sullivan. "Adaptive Spindle Balancing Using Magnetically Levitated Bearings." In *International Mechanical Engineering Congress and Expo, 1999*, November 1999.

[BPA12] Jeffrey A. Butterworth, Lucy Y. Pao, and Daniel Y. Abramovitch. "Analysis and Comparison of Three Discrete-Time Feedforward Model-Inverse Control Techniques for Nonminimum-phase Systems." *Mechatronics*, **22**(5):577–587, August 2012.

[BWS12] H.M.N.K. Balini, Jasper Witte, and Carsten W. Scherer. "Synthesis and Implementation of Gain-Scheduling and LPV Controllers for an AMB System." *Automatica*, **48**(3):521–527, March 2012.

[CDD94] L.Y. Cheung, Roderick W. Dunn, A.R. Daniels, and Tom Berry. "Active Vibration Control of Rotor Systems." In *Control, 1994. Control '94. International Conference on*, volume 2, pp. 1157–1163, March 1994.

[CJL10] Xiaofei Chen, Li Ji, and Kun Liu. "A BP Neural Network Controller for Magnetic Suspended Flywheel System." In *Computer Science and Information Technology (ICCSIT), 2010 3rd IEEE International Conference on*, volume 6, pp. 448–452, 2010.

[CT14] Herrick L. Chang and Tsu Chin Tsao. "High-Sampling Rate Dynamic Inversion - Filter Realization and Applications in Digital Control." *Mechatronics, IEEE/ASME Transactions on*, **19**(1):238–248, February 2014.

[CWW10] Kevin Chu, Yigang Wang, Jason Wilson, Chi Ying Lin, and Tsu Chin Tsao. "Modeling and Control of a Magnetic Bearing System." In *American Control Conference, 2010. ACC '10.*, pp. 2206–2211, June 2010.

[FW76] B.A. Francis and W.M. Wonham. "The Internal Model Principle of Control Theory." *Automatica*, **12**(5):457–465, September 1976.

[GL07] Thomas Grochmal and Alan F. Lynch. "Precision Tracking of a Rotating Shaft With Magnetic Bearings by Nonlinear Decoupled Disturbance Observers." *Control Systems Technology, IEEE Transactions on*, **15**(6):1112–1121, November 2007.

[HBG96] Raoul Herzog, Philipp Bühler, Conrad Gähler, and René Larsonneur. "Unbalance Compensation Using Generalized Notch Filters in the Multivariable Feedback of Magnetic Bearings." *Control Systems Technology, IEEE Transactions on*, **4**(5):580–586, September 1996.

[HST06] Hideo Hoshi, Tadahiko Shinshi, and Setsuo Takatani. "Third-generation Blood Pumps With Mechanical Noncontact Magnetic Bearings." *Artificial Organs*, **30**(5):324–338, May 2006.

[KHF95] Carl R. Knospe, Richard W. Hope, Stephen J. Fedigan, and Ronald D. Williams. "Experiments in the Control of Unbalance Response Using Magnetic Bearings." *Mechatronics*, **5**(4):385–400, June 1995.

[KHT96] Carl R. Knospe, Richard W. Hope, S.M. Tamer, and Stephen J. Fedigan. "Robustness of Adaptive Unbalance Control of Rotors with Magnetic Bearings." *Journal of Vibration and Control*, **2**(1):33–52, January 1996.

[KT14] Christopher Kang and Tsu Chin Tsao. "Control of Magnetic Bearings with Plug-in Time-Varying Harmonic Resonators." In *American Control Conference, 2014. ACC '14.*, pp. 4237–4242, June 2014.

[LCB08] Bei Lu, Heeju Choi, Gregory D. Buckner, and Kari Tammi. "Linear Parameter-Varying Techniques for Control of a Magnetic Bearing System." *Control Engineering Practice*, **16**(10):1161–1172, October 2008.

[LCR05] Ioan D. Landau, Aurelian Constantinescu, and Daniel Rey. "Adaptive Narrow Band Disturbance Rejection Applied to an Active Suspension - An Internal Model Principle Approach." *Automatica*, **41**(4):563–574, April 2005.

[Li97] Gang Li. "A Stable and Efficient Adaptive Notch Filter for Direct Frequency Estimation." *Signal Processing, IEEE Transactions on*, **45**(8):2001–2009, August 1997.

[LVK96] Timo I. Laakso, Vesa Valimaki, Matti Karjalainen, and Unto K. Laine. "Splitting the unit delay [FIR/all pass filters design]." *Signal Processing Magazine, IEEE*, **13**(1):30–60, January 1996.

[MFO89] F. Matsumura, Masayuki Fujita, and C. Oida. "A Design of Robust Servo Controllers for an Unbalance Vibration in Magnetic Bearing

Systems." In *Magnetic Bearings*, pp. 319–326. Springer Berlin Heidelberg, 1989.

[MNH96] Fumio Matsumura, Toru Namerikawa, Kazuhiko Hagiwara, and Masayuki Fujita. "Application of Gain Scheduled H_∞ Robust Controllers to a Magnetic Bearing." *Control Systems Technology, IEEE Transactions on*, **4**(5):484–493, September 1996.

[PDA09] Goele Pipeleers, Bram Demeulenaere, Farid Al-Bender, Joris De Schutter, and Jan Swevers. "Optimal Performance Tradeoffs in Repetitive Control: Experimental Validation on an Active Air Bearing Setup." *Control Systems Technology, IEEE Transactions on*, **17**(4):970–979, July 2009.

[PDD08] Goele Pipeleers, Bran Demeulenaere, Joris De Schutter, and Jan Swevers. "Robust high-order repetitive control: Optimal performance trade-offs." *Automatica*, **44**(10):2628–2634, October 2008.

[PMS96] Brad Paden, Nancy Morse, and Roy Smith. "Magnetic Bearing Experiment for Integrated Teaching and Research Laboratories." In *Control Applications, 1996., Proceedings of the 1996 IEEE International Conference on*, pp. 421–425, September 1996.

[RPL09] Brian P. Rigney, Lucy Y. Pao, and Dale A. Lawrence. "Nonminimum Phase Dynamic Inversion for Settle Time Applications." *Control Systems Technology, IEEE Transactions on*, **17**(5):989–1005, September 2009.

[SBT94] Gerhard Schweitzer, Hannes Bleuler, and Alfons Traxler. *Active Magnetic Bearings - Basics, Properties and Applications of Active Magnetic Bearings*. Vdf Hochschulverlag, Zurich, 1994.

[SL09] Juan Shi and Wee Sit Lee. "Analytical Feedback Design via Interpolation Approach for the Strong Stabilization of a Magnetic Bearing System." In *Control and Decision Conference, 2009*, pp. 274–279, 2009.

[SNF06] Hiroki Seto, Toru Namerikawa, and Masayuki Fujita. "Experimental Evaluation on H_∞ DIA Control of Magnetic Bearings with Rotor Unbalance." In *10th International Symposium on Magnetic Bearings, Hotel du Parc, Martigny, Switzerland*, 2006.

[Ste02] Maarten Steinbuch. "Repetitive control for systems with uncertain period-time." *Automatica*, **38**(12):2103–2109, December 2002.

[TD98] William Thomson and Marie Dahleh. *Theory of Vibration with Applications*. Prentice Hall, New Jersey, 5th edition, 1998.

[TGT13] Nolan Eizo Tsuchiya, James Steven Gibson, Tsu-Chin Tsao, and Michel Verhaegen. "Control of Jitter in a Laser Beam Experiment by Receding Horizon Adaptive Control." In *Mechatronic Systems*, pp. 383–390, April 2013.

[TGV13] Jonathan Tesch, Steve Gibson, and Michel Verhaegen. "Receding-horizon adaptive control of aero-optical wavefronts." *Optical Engineering*, **52**(7):071406–1–13, July 2013.

[THD07] Kari Tammi, Jari Hätönen, and Steve Daley. "Novel Adaptive Repetitive Algorithm for Active Vibration Control of a Variable-Speed Rotor." *Journal of Mechanical Science and Technology*, **21**(6):855–859, June 2007.

[Tom87] M. Tomizuka. "Zero Phase Error Tracking Algorithm for Digital Control." *Trans. of ASME, Journal of Dynamic Systems, Measurement, and Control*, **109**(1):65–68, March 1987.

[TQN98] Tsu Chin Tsao, Yao Xin Qian, and Mahadevamurty Nemani. "Repetitive Control for Asymptotic Tracking of Periodic Signals With an Unknown Period." *Journal of Dynamic Systems, Measurement, and Control*, **122**(2):364–369, February 1998.

[TTC89] Masayoshi Tomizuka, Tsu Chin Tsao, and Kok Kia Chew. "Analysis and Synthesis of Discrete-Time Repetitive Controllers." *Journal of Dynamic Systems, Measurement, and Control*, **111**(3):353–358, September 1989.

[WCT09a] Yigang Wang, Kevin Chu, and Tsu Chin Tsao. "Adaptive Control for Deterministic Trajectory Tracking and Random Disturbance Rejection with Application to Nano-Positioning of a Halback Linear Motor." In *ASME 2009 Dynamic Systems and Control Conference*, volume 2, pp. 581–588, October 2009.

[WCT09b] Yigang Wang, Kevin C. Chu, and Tsu Chin Tsao. "An analysis and synthesis of internal model principle type controllers." In *American Control Conference, 2009. ACC '09.*, pp. 488 –493, June 2009.

[WWZ07] Yigang Wang, Danwei Wang, Bin Zhang, and Keliang Zhou. "Fractional Delay Based Repetitive Control with Application to PWM DC/AC Converters." In *Control Applications, 2007. CCA 2007. IEEE International Conference on*, pp. 928–933, October 2007.

[YH00] Shiang Hwua Yu and Jwu Sheng Hu. "Asymptotic Rejection of Periodic Disturbances With Fixed or Varying Period." *Journal of Dynamic Systems, Measurement, and Control*, **123**(3):324–329, July 2000.

[YXS07] Guojun Yang, Yang Xu, Zhengang Shi, and Huidong Gu. "Characteristic Analysis of Rotor Dynamics and Experiments of Active Magnetic Bearing for HTR-10GT." *Nuclear Engineering and Design*, **237**(12-13):1363–1371, July 2007.

[ZD98] K. Zhou and J.C. Doyle. *Essentials of Robust Control*. Prentice-Hall, Inc., New Jersey, 1998.

[ZSL03] Xiaoyou Zhang, Tadahiko Shinshi, Lichuan Li, and Akira Shimokohbe. "A Combined Repetitive Control for Precision Rotation of Magnetic Bearing." *Precision Engineering*, **27**(3):273–282, July 2003.